IEEE Access
Multidisciplinary | Rapid Review | Open Access Journal

Received 18 February 2026, accepted 27 February 2026, date of publication 2 April 2026, date of current version 8 April 2026.

Digital Object Identifier 10.1109/ACCESS.2026.3680298

RESEARCH ARTICLE

Robust Speed Regulation of SPMSM Using Integral Terminal Sliding Mode and Novel Super-Twisting Extended State Observer

TRAN THANH TUYEN[1,2], JIAN YANG[1], (Member, IEEE), DAWEI NI[1,3], QILONG LIANG[1,4], AND NGUYEN GIA MINH THAO[5], (Senior Member, IEEE)

[1]School of Automation, Central South University, Changsha 410083, China
[2]Faculty of Electrical Engineering, Quang Ninh University of Industry, Mao Khe, Quang Ninh 200000, Vietnam
[3]Software Department of Research and Development Center, Shenzhen Huacheng Industrial Control Co., Ltd., Shenzhen 518126, China
[4]Precision Motion Control Research and Development Department, Maxwell Technology Co., Ltd., Zhuhai 519085, China
[5]Department of Mechanical, Electrical and Electronic Engineering, Shimane University, Matsue 690-8504, Japan

Corresponding authors: Jian Yang (jian.yang@csu.edu.cn) and Nguyen Gia Minh Thao (nguyenthao@riko.shimane-u.ac.jp)

This work was supported in part by the National Natural Science Foundation of China under Grant 52477071, in part by the Open Fund of State Key Laboratory of High-Efficiency and High-Quality Conversion for Electric Power under Grant 2024KF001, and in part by the Japan Society for the Promotion of Science (JSPS) KAKENHI under Grant 25K07797.

ABSTRACT This paper presents a proposed Sliding Mode Control (SMC) strategy for Surface-mounted Permanent Magnet Synchronous Motor (SPMSM) drives. The strategy integrates an Integral-type Terminal Sliding Mode Surface (ITSMS) with a Novel Super-Twisting Extended State Observer (NSTESO) to significantly enhance system robustness and dynamic performance. In detail, the ITSMS ensures finite-time stability and improves transient response under varying load conditions, while the NSTESO accurately estimates and compensates for time-varying disturbances, parameter uncertainties, and unmodeled dynamics. Moreover, a Novel Sliding Mode Reaching Law (NSMRL) is formulated using a hyperbolic tangent function instead of the conventional sign function, effectively reducing chattering while maintaining fast and smooth convergence. The proposed approach achieves excellently balanced trade-off between high-speed precision and control efficiency, and its stability is proven through Globally Asymptotically Stable (GAS) Lyapunov functions for both observer-free and observer-based configurations. Numerous simulation and experimental results under different operating conditions validate the superiority of the proposed NSMRL+NSTESO scheme in terms of speed tracking, overshoot reduction, disturbance rejection, and current regulation compared with existing SMC schemes, demonstrating that it can provide a feasible, reliable and high-performance control solution for SPMSM drives with strong robustness against disturbances and uncertainties.

INDEX TERMS Sliding mode control, integral-type terminal sliding mode surface (ITSMS), novel super-twisting extended state observer (NSTESO), novel sliding mode reaching law (NSMRL), SPMSM drives.

NOMENCLATURE

SMC	Sliding Mode Control.
PMSM	Permanent Magnet Synchronous Motor.
SPMSM	Surface-mounted Permanent Magnet Synchronous Motor.
ITSMS	Integral-Type Terminal Sliding Mode Surface.
NSTESO	Novel Super-Twisting Extended State Observer.
NSMRL	Novel Sliding Mode Reaching Law.
TERL	Traditional Exponential Reaching Law.
HOSMESO	High-Order Sliding-Mode-based Extended State Observer.

The associate editor coordinating the review of this manuscript and approving it for publication was Mouquan Shen.

FOC	Field-Oriented Control.
MPC	Model Predictive Control.
FLC	Fuzzy Logic Control.
i_d	d–axis stator current.
i_q	q–axis stator current.
u_d	d–axis stator voltage.
u_q	q–axis stator voltage.
R_s	Stator winding resistance.
L	Stator synchronous inductance.
ψ_f	Permanent-magnet flux linkage.
ω_e	Electrical angular speed.
ω_m	Mechanical angular speed.
T_e	Electromagnetic torque.
T_L	Load torque.
ASMC	Adaptive Sliding Mode Controller.
GAS	Globally Asymptotically Stable.
MVERL	Modified Variable Exponential Reaching Law.
SMSs	Sliding Mode Surfaces.
SMDOs	Sliding Mode Disturbance Observers.
FTSTDOs	Finite-Time Super-Twisting Disturbance Observers.
ESOs	Extended State Observers.
INFTSM	Improved Nonsingular Fast Terminal Sliding Mode.
t_{TERL} and t_{NSMRL}	The reaching times of the TERL and the NSMRL.
k_1	Positive variable-speed reaching law of gains.
k_2	Positive variable-index reaching law of gains.
$d(t)$ and $D(t)$	The external disturbance.
a_1, a_2 and a_3	Super-twisting observer gains.
Ω_m	Motor output speed.
J	Rotor moment of inertia.
B	Viscous damping coefficient.
p	Number of pole pairs.
η	Torque constant.
σ, λ and μ	Exponent gains.
α and β	Positive constants.
$u(t)$	Control input.
e	Speed error.
χ	Positive sliding gain.
s	Sliding surface (sliding variable).
x	The system state.

I. INTRODUCTION

Surface-mounted Permanent Magnet Synchronous Motors (SPMSMs) are widely employed in industrial and consumer applications, such as robotic arms [1] and Electric Vehicle (EV) [2], [3], due to their advantages of high efficiency, high power density, and precise control capability [4], [5]. However, SPMSMs present certain control challenges, as they are inherently nonlinear and strongly coupled systems [6], [7]. To achieve satisfactory dynamic performance, various control schemes have been applied to PMSMs, such as Field-Oriented Control (FOC) [8], [9]. The FOC strategy employs two nested loops: an outer speed loop and an inner current loop. The outer loop governs the speed response and generates the reference for the inner loop, while the inner loop directly affects the overall dynamic behavior of the drive system. In many studies, the design of the outer speed loop is given particular attention, as it plays a crucial role in ensuring accurate tracking performance and strong disturbance rejection for PMSM drives.

When conventional linear controllers, such as Proportional-Integral (PI) schemes [10], are applied, the control accuracy is generally limited to a narrow operating range. To overcome these limitations, several advanced control strategies have been introduced to improve the performance of the speed loop, including Model Predictive Control (MPC) [11], Sliding Mode Control (SMC) [12] and Fuzzy Logic Control (FLC) [13]. Among these, SMC is often preferred because of its robustness to parameter variations and strong resistance to internal and external disturbances.

The SMC strategy has received considerable attention as an effective nonlinear control method for PMSM drives [14]. Its fundamental principle is to regulate the system dynamics toward a predefined low-order sliding surface using discontinuous switching control. SMC provides several advantages, including strong robustness against model uncertainties, parameter variations, and system nonlinearities [15]. Because this approach does not rely heavily on an accurate system model, it is well-suited for a wide range of practical motor-drive applications. Numerous improvements have been proposed for SMC controllers, such as enhanced sliding mode control law designs [16], higher-order SMC schemes [17], and observer-based techniques [9], [18]. In particular, SMC designs incorporating novel sliding approach laws combined with nonlinear sliding surfaces are commonly employed to mitigate the chattering phenomenon [19]. Due to their relatively simple design and low computational requirements, these methods have been extensively studied in recent years. In addition, to improve chattering resistance, the sign function can be replaced with smoothing alternatives such as the hyperbolic tangent function [20], continuous sigmoid function [21] and saturation function [22], thereby enhancing the output speed performance of the SMC-based control system for PMSM drives.

The SMC control model with Adaptive Sliding Mode Control (ASMC) [23] is developed to improve PMSM speed regulation. It effectively reduces chattering, shortens reaching time, and enhances disturbance rejection as well as speed-jump stability. However, it still neglects torque ripple, exhibits limited performance under high-frequency disturbances, and requires careful parameter tuning for extreme operating conditions. Similarly, the SMC control model with Modified Variable Exponential Reaching Law (MVERL) [24] incorporates advanced techniques to achieve finite-time convergence, strong disturbance rejection, and effective chattering suppression. Nevertheless, it remains sensitive to harmonic disturbances under heavy loads, depends on precise parameter tuning, and entails high computational complexity.

Beyond the reaching law design, the selection of the Sliding Mode Surfaces (SMSs) also plays a critical role in improving tracking accuracy and disturbance rejection. The SMSs for PMSM drives and nonlinear systems have focused on addressing limitations of conventional linear SMSs (e.g., steady-state errors) and standard terminal SMSs (e.g., singularity, insufficient disturbance rejection) [9], [15], [24]. Approaches include integrating integral terms, non-singular terminal functions, and adaptive gains to enhance convergence speed, robustness, and chattering suppression [4], [19]. The Integral-type Terminal Sliding Mode Surface (ITSMS) is preferred over other surfaces for its ability to eliminate steady-state errors via integral error compensation, achieve finite-time convergence without singularity, and strengthen disturbance rejection by integrating cumulative uncertainties [9], [24]. When combined with SMC, ITSMS synergizes with disturbance observers and modified reaching laws to outperform linear SMSs and standard terminal SMSs in dynamic response and robustness for PMSM control.

From an anti-disturbance control perspective, in addition to observer-based methods, various anti-disturbance frameworks, including performance-guaranteed and event-triggered strategies, have also been investigated in non-linear control systems. However, for high-performance PMSM drives, observer-based approaches integrated with sliding-mode control remain widely adopted due to their simplicity, fast response, and robustness. Accordingly, recent research on observers for PMSM drives has focused on finite-time convergence, chattering suppression, and multi-disturbance estimation, with Sliding Mode Disturbance Observers (SMDOs) [4], Finite-Time Super-Twisting Disturbance Observers (FTSTDOs) [16], and Super-Twisting Extended State Observer (STESO) [24]. These observers address parameter uncertainties, external loads, and harmonic disturbances but often face trade-offs between estimation speed, noise immunity, or complexity [15], [18]. The STESO is chosen over other observers for its integration of super-twisting technology and Extended State Observer (ESO) advantages, enabling fast finite-time convergence of disturbance estimation errors while reducing chattering, without relying on precise system models [24]. Structurally, the proposed STESO (a super-twisting-based ESO) can be interpreted as an extension of the classical ESO augmented with a super-twisting algorithm, which preserves the lumped disturbance estimation framework of ESO while introducing finite-time convergence and enhanced robustness against disturbances. When combined with an Improved Nonsingular Fast Terminal Sliding Mode (INFTSM) controller, this STESO-based composite scheme outperforms conventional observers (e.g., SMDOs, ESOs) in disturbance rejection and dynamic response for PMSM speed regulation.

To address the limitations identified in previous studies, this paper proposes a novel SMC law that incorporates a nonlinear sliding surface together with a High-Order Sliding-Mode-based Extended State Observer (HOSMESO) for an advanced SMC controller. The proposed method effectively suppresses chattering while simultaneously reducing the convergence time required for the system states to reach the sliding surface. The main contributions of this work are summarized as follows:

- A new SMC approach is proposed, featuring a Novel Sliding Mode Reaching Law (NSMRL) that incorporates an enhanced strategy using a hyperbolic tangent (tanh) function instead of the conventional sign-switching function, together with an ITSMS that adapts to variations in both the sliding surface and the system state. Besides, its convergence is rigorously proven through Lyapunov analysis, and the proposed method achieves faster convergence than traditional approaches.
- In addition, a new HOSMESO-based sliding-mode speed controller—the Novel Super-Twisting Extended State Observer (NSTESO)—is introduced to obtain strong dynamic performance and robust disturbance rejection under speed uncertainties. Furthermore, its theoretical stability is confirmed by using Globally Asymptotically Stable (GAS) Lyapunov functions for both the observer-free and observer-based configurations.
- To evaluate the effectiveness of the proposed control strategy (NSMRL+NSTESO), a comparative analysis is conducted against three controllers: the conventional SMC, the ASMC-based controller, and the controller using the MVERL law. The proposed controller is also compared with its variant using the sign function, as well as with different coefficient values of the hyperbolic tangent function. Finally, simulations and experiments under various operating cases demonstrate the robustness and efficacy of the proposed strategy.

The remainder of this paper is structured as follows. Section II describes the SPMSM dynamic model and derives the proposed NSMRL control law. Section III presents performance analysis, stability proof, and design of the SMC controller using the NSMRL-integrated ITSMS. Then, Section IV introduces the proposed NSTESO architecture, while Section V provides a comprehensive stability assessment of the combined NSMRL+NSTESO system. Section VI provides many simulation and experimental results, as well as relevant detailed comparisons and discussions. Finally, Section VII concludes this paper and briefly indicates future directions of the research.

II. MATHEMATICAL MODEL SPMSM AND NOVEL SLIDE MODE LAW

A. MATHEMATICAL MODEL OF SPMSM

The mathematical model of the SPMSM, formulated in the synchronous rotating $d-q$ reference frame [25] is defined as follows:

$$\frac{di_d}{dt} = \frac{1}{L}\left(u_d - R_s i_d + \omega_e L i_q\right) \tag{1}$$
$$\frac{di_q}{dt} = \frac{1}{L}\left(u_q - R_s i_q - \omega_e L i_d - \omega_e \psi_f\right) \tag{2}$$
$$\frac{d\omega_m}{dt} = \frac{1}{J}\left(T_e - B\omega_m - T_L\right) \tag{3}$$
$$T_e = \frac{3}{2} p\psi_f i_q = \eta i_q \tag{4}$$

Here, $\eta = 1,5p\psi_f$, u_d, u_q, i_d, and i_q denote the voltages (V) and currents (A) along the d-axis and q-axis in the d-q reference frame, respectively; R_s is the stator winding resistance (Ω); ω_e and ω_m are the electrical angular speed (rad/s) and the mechanical angular speed (rad/s), respectively; L is the synchronous inductance of the stator winding (H). Furthermore, ψ_f is the flux linkage generated by the permanent magnets (Wb); T_L and T_e are the load torque (Nm) and the electromagnetic torque (Nm), respectively; p is number of pole-pairs of the electric motor; J and B represent the rotor moment of inertia (kg·m^2) and the damping coefficient (Ns/m), respectively.

Combining Eq. (3) and Eq. (4) gives:

$$J\dot{\omega}_m = \eta i_q - B\omega_m - T_L \tag{5}$$

From Eq. (5), it is observed that the SPMSM is sensitive to internal parameters, for example, inertia and damping coefficients, while also being influenced by external factors such as load torque. This poses a challenge in balancing response speed and stability when applying the SMC controller to the motor. This paper proposes a novel control law that not only ensures system stability and fast convergence under uncertainties, but also simultaneously improves the dynamic response and steady-state stability of the SPMSM drive during operation.

B. NOVEL SLIDING MODE REACHING LAW FOR CHATTERING REDUCTION

The derivative of the SMS function is (Traditional Exponential Reaching Law, TERL):

$$\dot{s} = -k_1 sign\,(s) - k_2 s k_1, k_2 > 0 \tag{6}$$

When the system reaches the sliding surface, for example, $s(0) = s_0$ and $s(t) = 0$, the reaching time of the TERL can be determined as:

$$t_{TERL} = \frac{1}{k_2}\left\{\ln\left[s_0 + \frac{k_1}{k_2}\right] - \ln\left(\frac{k_1}{k_2}\right)\right\} \tag{7}$$

From Eq. (7), it can be observed that k_2 is the reaching coefficient that determines the approaching speed of the system to the sliding surface; as its value increases, the reaching time TERL decreases toward zero, indicating a faster reaching speed. However, a larger k_2 results in increased chattering once the system reaches the sliding surface. Therefore, a sliding mode reaching law is as follows:

$$\begin{cases} \dot{s} = -k_1 F(s,t) sign\,(s) - k_2 G(x,t) s \\ F(s,t) = 1 + e^{-\alpha|s|}(1-\beta)\big/\beta, \quad 1 > \beta > 0, \alpha > 0 \\ G(x,t) = |x|^{\sigma}\big/(|x|+1), \quad k_1, k_2, \sigma > 0, \lim\limits_{t\to\infty} |x| = 0 \end{cases} \tag{8}$$

where x represents the system state.

In the system, the state converges to the SMS according to two distinct reaching laws: the variable-speed reaching law and the variable-index reaching law. In the conventional variable-speed reaching law, *F(s,t)* acts as an auxiliary term within the sign coefficient, helping to accelerate convergence and reduce the settling time of the system states. For the variable-index reaching law, *G(x,t)* is introduced to adaptively modify the control gain, thereby enhancing the robustness and precision of the sliding-mode performance under varying load conditions and external disturbances. Together, these functions ensure faster convergence, lower chattering, and improved overall stability of the SMC system.

When the sliding variable magnitude $|s|$ is large (indicating the system state is far from the sliding surface), the adaptive gain satisfies k_1*F(s,t)* ≈ $k_1\{1+(1)-\beta)/\beta\}$, resulting in a high-gain control effort. This ensures rapid convergence of the system state trajectory toward the sliding surface. Conversely, when $|s|$ is small (near the sliding surface), the gain *F(s,t)* reduces to k_1, establishing a low-gain regime. This reduction in gain effectively suppresses control chattering while preserving closed-loop stability. The term k_1*F(s,t)* provides dynamic gain adjustment, guaranteeing the finite-time convergence to the sliding surface $s = 0$; optimal balance between transient performance (fast reaching phase) and steady-state precision (smooth sliding phase).

The state-dependent linear term k_2*G(x,t)* exhibits the following characteristics: when $|x|$ is relatively large, k_2*G(x,t)* $\approx k_2|x|^{\sigma-1}$, which increases the influence of this term on the dynamics *ds/dt*, accelerating the movement of the system state towards the SMS; when $|x|$ is small, k_2*G(x,t)* $\approx k_2|x|^{\sigma}$ is also small, reduces the control effort and helping to avoid overshoot and chattering near the SMS.

It can be observed that the speed variation component includes the sign function, which is simple and computationally efficient. However, the abrupt switching behavior of this function leads to chattering in the controller. To overcome this drawback, various methods have been proposed to reduce or eliminate chattering in SMC systems [14].

The hyperbolic tangent function $\tanh(\varepsilon s)$ [14] smooths the state transition and mitigates chattering, expressed as:

$$\tanh(\varepsilon s) = \frac{e^{\varepsilon s} - e^{-\varepsilon s}}{e^{\varepsilon s} + e^{-\varepsilon s}}, \varepsilon > 0 \tag{9}$$

Several continuous switching functions, such as the sigmoid, saturation, and hyperbolic tangent functions, can significantly reduce chattering in the system. As shown in Fig. 1, the hyperbolic tangent function not only mitigates the

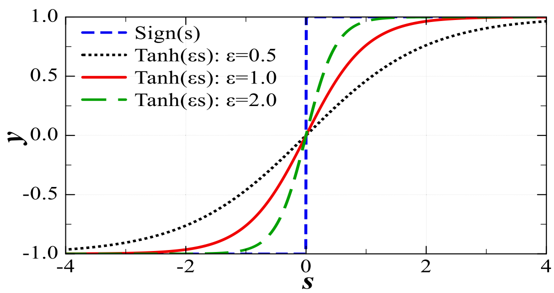

FIGURE 1. **Comparative analysis between the hyperbolic tangent function and the sign function.**

chattering caused by abrupt switching but also ensures a fast response during the transient phase. Therefore, the authors propose a Novel Sliding Mode Reaching Law (NSMRL) law as follows:

$$\begin{cases} \dot{s} = -k_1 F(s,t)\tanh(\varepsilon s) - k_2 G(x,t)s \\ F(s,t) = 1 + e^{-\alpha|s|}(1-\beta)\big/\beta, \quad 1 > \beta > 0, \alpha > 0 \\ G(x,t) = |x|^{\sigma}\big/(|x|+1), \quad k_1, k_2, \sigma, \varepsilon > 0, \lim\limits_{t\to\infty}|x| = 0 \end{cases} \tag{10}$$

III. PERFORMANCE AND STABILITY ANALYSIS AND DESIGN OF SPEED CONTROLLER

A. PERFORMANCE ANALYSIS OF NSMRL

Consider the following second-order nonlinear system:

$$\begin{cases} \dot{x}_1 = x_2 \\ \dot{x}_2(t) = f(x,t) + \varphi u(t) + d(t) \quad \varphi > 0 \end{cases} \tag{11}$$

Here, $x = [x_1, x_2]$ are the state variables representing the position and speed of the motor, $f(x,t)$ is a nonlinear function, $u(t)$ is the control input, and $d(t)$ denotes the external disturbance.

The nonlinear function $f(x,t)$ is derived from a simplified model of the motor system dynamics, which can effectively capture the nonlinear characteristics of the system while maintaining simplicity and feasibility in control design. The coefficient φ represents the gain of $u(t)$, directly affecting its amplitude. A larger value of φ implies that the controller responds more sensitively to the system states, allowing faster reaction and adjustment. For mechanical systems, motor drives, or other dynamic systems, external disturbances are often periodic in nature, such as cyclic vibrations or load oscillations. Therefore, $d(t)$ is selected as a periodic disturbance to evaluate the impact of external periodic disturbances that the system may encounter during actual operation. Accordingly, the main controller parameters are set as: $f(x,t) = -25\ddot{x}$, $\varphi = 100$, $d(t) = 5\sin(\pi t)$.

Assume that x_d is the reference signal. Then, the error signal is defined as $e(t) = x_d - x_1$, and the sliding surface is chosen as follows:

$$s = \chi e(t) + \dot{e}(t)\chi > 0 \tag{12}$$

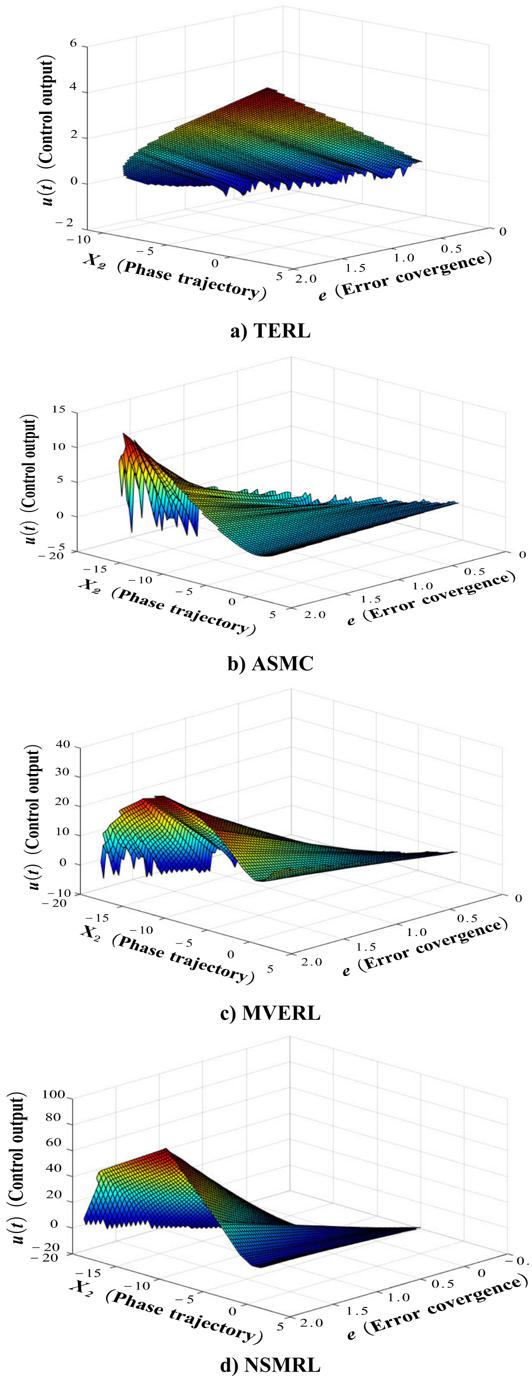

FIGURE 2. **Performance comparison TERL, ASMC, MVERL laws and proposed NSMRL law.**

From Eqs. (10), (11), and (12), the control signal of the system is obtained as follows:

$$u(t) = \frac{1}{\varphi}\left[k_1\left(1 + e^{-\alpha|s|}(1-\beta)\big/\beta\right)\tanh(\varepsilon s) + k_2\frac{|x|^{\sigma}}{|x|+1}s \right. \\ \left. +\chi(\dot{x}_d - \dot{x}) + \ddot{x}_d - f(x,t) - d(t)\right] \tag{13}$$

To evaluate the chattering reduction capability and performance of the proposed NSMRL, simulations are carried out in

MATLAB, comparing it with several existing reaching laws, including the AMSC [23], the TERL, the MVERL () [24] as well as the proposed NSMRL law.

Accordingly, the ASMC law [23] is given as follows:

$$\begin{cases} \dot{s} = -k_1 F(x,s) sign\,(s)\,, & k_1 > 0, \\ F(x,s) = |x| \dfrac{1+\beta - e^{-\alpha|s|}}{\beta}, & \alpha > 0, 1 > \beta > 0, \end{cases} \tag{14}$$

Accordingly, the MVERL law [24] is given as follows:

$$\begin{cases} \dot{s} = -k_1 F(x,s) sign\,(s) - k_2 G(x,t) s, & k_1, k_2 > 0, \\ F(x,s) = |x| \left[1 + \alpha\left(1 - e^{-\beta|s|}\right)\right], & \alpha > 1, \beta > 0, \\ G(x,t) = |x|^{\lambda} \quad 2 > \lambda > 0, \lim\limits_{t\to\infty} |x| = 0 \end{cases} \tag{15}$$

With the evaluation parameters set as: $k_1 = 25$, $k_2 = 25$, $\chi = 10$, $\alpha = 2$, $\beta = 0.5$, $\sigma = 2.5$ and $\lambda = 1.5$. The initial state of the controlled system is set to $x(0) = [-2, -2]$, and the reference signal is $x_d = \sin t$.

In Fig. 2, the performance of NSMRL law is compared with TERL, ASMC, and MVERL laws using several evaluation criteria. In terms of tracking performance, both NSMRL and MVERL laws closely follow the reference signal with high precision and minimal deviation. The control output of NSMRL law exhibits smoother behavior, significantly reduced chattering, and faster convergence to zero. The position error analysis indicates that NSMRL law achieves faster error reduction and better steady-state accuracy than the other methods. Regarding the phase trajectory response, the NSMRL law approaches the desired manifold more efficiently and with less overshoot. Overall, the NSMRL law demonstrates superior tracking accuracy, control smoothness, and transient performance, achieving an effective balance between fast response and steady-state precision.

B. STABILITY PROOF

The Lyapunov function can be constructed as follows:

$$L_1 = \frac{1}{2} s^2 \tag{16}$$

Combining Eq. (10) and Eq. (16), the derivation of Eq. (16) can be obtained as follows:

$$\begin{aligned} \dot{L}_1 = s\dot{s} &= s\left(-k_1\left(1 + \frac{1-\beta}{\beta} e^{-\alpha|s|}\right)\right. \\ &\quad \left. \tanh\,(\varepsilon s) - k_2 \frac{|x|^{\sigma}}{|x|+1} s\right) \\ &= -k_1 s\left(1 + \frac{1-\beta}{\beta} e^{-\alpha|s|}\right) \\ &\quad \tanh\,(\varepsilon s) - k_2 \frac{|x|^{\sigma}}{|x|+1} s^2 \end{aligned} \tag{17}$$

If $s > 0$, $1 > \beta > 0$, k_1, k_2, $\alpha > 0$, $\tanh(\varepsilon s) > 0$ then $-k_2 \frac{|x|^{\sigma}}{|x|+1} s^2 < 0$, $-k_1 s\left(1 + e^{-\alpha|s|} \frac{1-\beta}{\beta}\right) \tanh\,(\varepsilon s) < 0$, $\dot{L}_1 < 0$.

When $s < 0$, $\tanh(\varepsilon s) < 0$ then $-k_2 \frac{|x|^{\sigma}}{|x|+1} s^2 < 0$, $-k_1 s\left(1 + e^{-\alpha|s|} \frac{1-\beta}{\beta}\right) \tanh\,(\varepsilon s) < 0$, $\dot{L}_1 < 0$.

It is known from the Lyapunov stability theorem that the designed SMC is progressively stable.

C. CONVERGENCE OF NSMRL

Assuming the initial state $s_0 > 1$, the approach to the SMS can be divided into two stages: $s_0 \to s = 1$, and $s = 1 \to s = 0$. The corresponding reaching time is given by:

$$t_{NSMRL} = \int_0^{s_0} \frac{1}{k_1\left(1 + \frac{1-\beta}{\beta} e^{-\alpha|s|}\right) \tanh\,(\varepsilon s) + k_2 \frac{|x|^{\sigma}}{|x|+1} s} ds \tag{18}$$

If $s_0 > 0$, $\tanh(\varepsilon s) > 0$ with $s \in (0, s_0]$, an upper bound of the reaching time can be obtained by neglecting the nonnegative term $k_2 \frac{|x|^{\sigma}}{|x|+1} s$. Eq. (18) can be conservatively bounded as:

$$t_{s_0>0} < \int_0^{s_0} \frac{1}{k_1\left(1 + e^{-\alpha|s|} \frac{1-\beta}{\beta}\right)} ds \tag{19}$$

Evaluating the above integral gives:

$$t_{s_0>0} < \frac{\ln\left(1 + \beta\left(e^{\alpha s_0} - 1\right)\right)}{k_1 \alpha} \tag{20}$$

In Eq. (7), the reaching time of the TERL exhibits logarithmic, asymptotic convergence, which slows down for larger initial error s_0 and requires higher gains (k_1, k_2) to achieve faster responses. By contrast, the reaching time of the proposed NSMRL in Eq. (20) guarantees finite-time convergence, with an explicitly bounded duration that scales with the exponential of the initial state $e^{\alpha s_0}$. This allows NSMRL to reach the sliding surface more quickly, especially for large initial deviations. Furthermore, its state-dependent design enables adaptive control, minimizing chattering and reducing control effort compared to TERL. Overall, NSMRL exhibits superior performance in terms of convergence speed, predictability, and robustness.

D. NOVEL DESIGN OF INTEGRAL-TYPE TERMINAL SLIDING MODE SURFACE

The SMC speed control is implemented using the designed NSMRL law, driving the system states from arbitrary initial conditions to a predefined sliding surface. This ensures that the actual motor speed closely tracks the reference, with the speed-tracking error selected as a system state variable. For analytical convenience, the following definition is introduced:

$$\begin{cases} x_1 = \omega_{ref} - \omega_m \\ x_2 = \dot{x}_1 = \dot{\omega}_{ref} - \dot{\omega}_m \end{cases} \tag{21}$$

where, ω_{ref} and ω_m denote the reference speed and the actual system speed, respectively.

Considering the effect of disturbances during actual operation, Eqs. (5) and (21) can be rewritten as:

$$x_2 = -\frac{\eta}{J} i_q^* - \frac{B}{J}\omega_m + D(t) \tag{22}$$

where i_q^* denotes the reference q-axis current, and $D(t)$ represents the external disturbance, which can be formulated as:

$$D(t) = \frac{\eta}{J} i_q - \frac{T_L}{J} + \frac{\eta}{J} i_q^* \tag{23}$$

The Integral-type Terminal Sliding Mode Surface (ITSMS) function [19] is:

$$s = x_1 + C\int_0^t |x_1|^{\mu}\, sign(x_1) dt \tag{24}$$

where $C > 0$, $1 > \mu > 0$. Differentiating Eq. (24), it can be obtained that:

$$\dot{s} = x_2 + C|x_1|^{\mu}\, sign(x_1) \tag{25}$$

From Eq. (22) and Eq. (25), then:

$$\dot{s} = \left(-\frac{\eta}{J} i_q^* - \frac{B}{J}\omega_m + D(t)\right) + C|x_1|^{\mu}\, sign(x_1) \tag{26}$$

$$i_q^* = \frac{J}{\eta}\left[-\dot{s} - \frac{B}{J}\omega_m + D(t) + C|x_1|^{\mu}\, sign(x_1)\right] \tag{27}$$

To achieve enhanced dynamic performance and improved tracking, a sliding mode controller employing the ITSMS surface is adopted. Based on the novel sliding mode law in Eq. (10), the q-axis current under the NSMRL+ITSMS scheme is given by:

$$\begin{aligned} i_q^* &= \frac{J}{\eta}\left[k_1\left(1 + \frac{1-\beta}{\beta}e^{-\alpha|s|}\right)\right. \\ &\left.\tanh(\varepsilon s) + k_2\frac{|x|^{\sigma}}{|x|+1}s + C|x_1|^{\mu}\, sign(x_1) - \frac{B}{J}\omega_m + D(t)\right] \\ &= \frac{J}{\eta}\left[k_1\left(1 + \frac{1-\beta}{\beta}e^{-\alpha|s|}\right)\right. \\ &\left.\tanh(\varepsilon s) + k_2\frac{|x|^{\sigma}}{|x|+1}s + C|x_1|^{\mu}\, sign(x_1) - \frac{B}{J}\omega_m\right] \\ &+ \frac{J}{\eta}D(t) = i_{NSMRL} + \frac{J}{\eta}D(t) \end{aligned} \tag{28}$$

Here, $i_{NSMRL}\mathrm{i_{qn}}$ represents the control signal without accounting for the system's external load disturbance, while $D(t)$ includes the external disturbance such as load torque. The block diagram of the speed controller employing the new reaching law is shown in Fig. 3.

To improve the dynamic performance of the three-phase SPMSM drive system, the NSMRL law is implemented using the ITSMS surface method, leading to the controller expression presented in Eq. (28). As shown in Eq. (28), the integral term in the controller plays a dual role: it mitigates oscillations and eliminates steady-state error, thereby enhancing the overall control quality of the system.

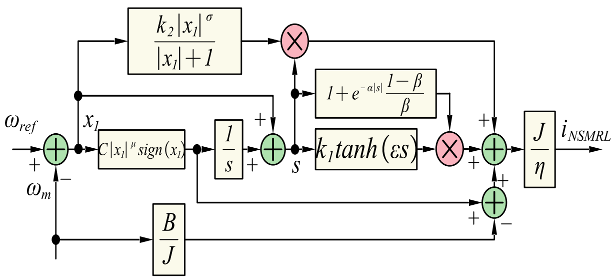

FIGURE 3. Model simulates the SMC controller according to ITSMS surface with NSMRL law.

IV. DESIGN OF NOVEL SUPER-TWISTING EXTENDED STATE OBSERVER

When designing the SMC scheme, the disturbance $D(t)$ which mainly corresponds to the load disturbance and is typically assumed to be constant, is required. However, this disturbance is difficult to obtain in practical applications. Therefore, a Novel Super-Twisting Extended State Observer (NSTESO) is introduced to estimate $D(t)$. Based on Eq. (3), the SPMSM speed system is formulated as follows:

$$\begin{cases} \dot{\omega}_m = \frac{\eta}{J} i_q - \frac{B}{J}\omega_m + D(t) \\ \dot{D}(t) = d(t) \quad |D(t)| \le D_{\max} \end{cases} \tag{29}$$

where $D(t)$ is the disturbance and bounded, D_{max} is a constant.

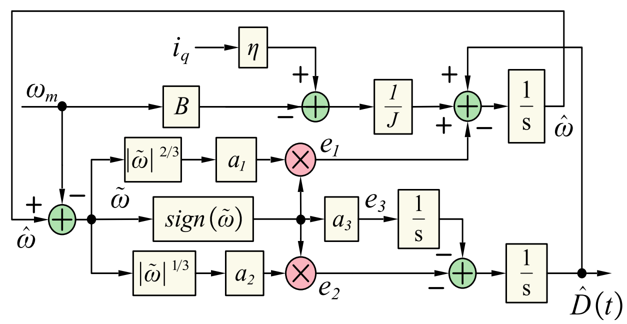

FIGURE 4. Block diagram of the NSTESO.

In order to estimate the total disturbance and compensate for it, the NSTESO designed for Eq. (29) can be as:

$$\begin{cases} \tilde{\omega} = \hat{\omega} - \omega_m \\ \dot{\hat{\omega}} = \frac{\eta}{J} i_q - \frac{B}{J}\omega_m + \hat{D}(t) - e_1(\tilde{\omega}) \\ \dot{\hat{D}}(t) = \hat{d}(t) - e_2(\tilde{\omega}) \\ \dot{\hat{d}}(t) = -e_3(\tilde{\omega}) \end{cases} \tag{30}$$

where $\tilde{\omega}$ is the speed tracking error, $\hat{\omega}$ and $\hat{D}(t)$ are the estimated values of the state variables ω and $D(t)$ respectively. To observe the state variables in Eq. (31), a generalized super-twisting algorithm [26] is constructed as follows:

$$\begin{cases} e_1(\tilde{\omega}) = a_1 |\tilde{\omega}|^{2/3} sign(\tilde{\omega}) \\ e_2(\tilde{\omega}) = a_2 |\tilde{\omega}|^{1/3} sign(\tilde{\omega}) \\ e_3(\tilde{\omega}) = a_3 sign(\tilde{\omega}) \end{cases} \quad (31)$$

where a_1, a_2 and $a_3 > 0$.

By reformulating state Eq. (31), the system dynamics can be expressed as:

$$\begin{cases} \tilde{\omega} = \hat{\omega} - \omega_m \\ \dfrac{d\hat{\omega}}{dt} = \dfrac{\eta}{J} i_q - \dfrac{B}{J}\omega_m + \hat{D}(t) - a_1 |\tilde{\omega}|^{2/3} sign(\tilde{\omega}) \\ \dfrac{d\hat{D}(t)}{dt} = \hat{d}(t) - a_2 |\tilde{\omega}|^{1/3} sign(\tilde{\omega}) \\ \dfrac{d\hat{d}(t)}{dt} = -a_3 sign(\tilde{\omega}) \end{cases} \quad (32)$$

The structural block diagram of the NSTESO is illustrated in Fig. 4, providing a detailed overview of its internal configuration and functional components.

V. COMPREHENSIVE STABILITY ASSESSMENT OF PROPOSED NSMRL + NSTESO SYSTEM

This section presents a unified stability analysis of the NSMRL combined with the ITSMS under two scenarios: with and without the NSTESO.

A. WITHOUT NSTESO

Once NSTESO is not used, the speed tracking error $\tilde{\omega}$ is as:

$$\tilde{\omega} = \omega_{ref} - \omega_m \quad (33)$$

The SPMSM dynamics under disturbance in Eq. (22) and Eq. (24) become:

$$\dot{\omega}_m = -\frac{\eta}{J} i_q^* - \frac{B}{J}\omega_m + D(t) \quad (34)$$

$$s = \tilde{\omega} + C\int_0^t |\tilde{\omega}|^{\mu} sign(\tilde{\omega}) dt \quad (35)$$

By differentiating Eq. (35) and combining it with Eqs. (33) and (34), the following expression is obtained:

$$\dot{s} = \left(\dot{\omega}_{ref} - \frac{\eta}{J} i_q^* - \frac{B}{J}\omega_m + D(t)\right) + C|\tilde{\omega}|^{\mu} sign(\tilde{\omega}) \quad (36)$$

The NSMRL is designed to impose the desired sliding dynamics that drive s toward zero while explicitly accounting for $D(t)$:

$$\dot{s} = -k_1 F(s,t) \tanh(\varepsilon s) - k_2 G(x,t) s + D(t) \quad (37)$$

The q-axis current under the NSMRL+ITSMS scheme is given by:

$$i_q^* = \frac{J}{\eta}\Big[k_1 F(s,t) \tanh(\varepsilon s) + k_2 G(x,t) s + C|\tilde{\omega}|^{\mu} sign(\tilde{\omega}) - \frac{B}{J}\omega_m + D(t)\Big] \quad (38)$$

Once reach the SMS $s = 0$, Eq. (35) becomes:

$$\tilde{\omega} + C\int_0^t |\tilde{\omega}|^{\mu} sign(\tilde{\omega}) dt = 0 \quad (39)$$

Meanwhile, it can be shown that $\dot{s} = 0$:

$$\dot{\tilde{\omega}} + C|\tilde{\omega}|^{\mu} sign(\tilde{\omega}) = 0 \quad (40)$$

It follows that:

$$\dot{\tilde{\omega}} = -C|\tilde{\omega}|^{\mu} sign(\tilde{\omega}) \quad (41)$$

Lyapunov function [27] that explicitly incorporates the ITSMS:

$$L_2 = \frac{1}{2}s^2 + \frac{C}{1+\mu}|\tilde{\omega}|^{1+\mu} \quad (42)$$

The time derivative of L_2, with respect to time and using Eq. (41) yields:

$$\dot{L}_2 = s\dot{s} + C|\tilde{\omega}|^{\mu} sign(\tilde{\omega})\dot{\tilde{\omega}} = A + B \quad (43)$$

With B:

$$B = C|\tilde{\omega}|^{\mu} sign(\tilde{\omega})\left[-C|\tilde{\omega}|^{\mu} sign(\tilde{\omega})\right] = -C^2|\tilde{\omega}|^{2\mu} < 0 C > 0 \quad (44)$$

With A:

$$\begin{aligned} A &= s\dot{s} \\ &= s\left[-k_1 F(s,t) \tanh(\varepsilon s) - k_2 G(x,t) s + D(t)\right] \\ &= \dot{L}_1 + sD(t) \end{aligned} \quad (45)$$

As shown above, $\dot{L}_1 < 0$; therefore, $\dot{L}_2 < 0$for $sD(t) < 0$. Bound using:

$$sD(t) \le |s| D_{\max} D_{\max} = \sup|D(t)| \quad (46)$$

For $\dot{L}_2 < 0$:

$$|s| D_{\max} < k_1 F(s,t) s \tanh(\varepsilon s) + k_2 G(x,t) s^2 \quad (47)$$

If |s| very large, hence $F(s,t) \to 1$(since $e^{-\alpha|s|} \to 0$); $s\tanh(\varepsilon s) \to |s|$ (since $\tanh(\varepsilon s) \to$sign(s)); $G(x,t) \to |x|^{\sigma-1} \to 0$. However, $k_1 F(s,t) s\tanh(\varepsilon s) \to k_1|s|$, which dominates $|s| D_{\max}$ if $D_{\max} < k_1$.

If |s| very small, hence $F(s,t) \to 1 + (1-\beta)/\beta = 1/\beta > 1$(since $1 > \beta > 0$); $s\tanh(\varepsilon s) \approx \varepsilon s^2$ (since $\tanh(\varepsilon s) \approx \varepsilon s$). Thus, $k_1 F(s,t) s\tanh(\varepsilon s) \approx k_1 \varepsilon s^2/\beta$; therefore, which dominates $|s| D_{\max}$ for small $|s|$.

The Lyapunov function L_2 is positive definite, and its derivative satisfies $\dot{L}_2 < 0$for all $s \neq 0$ provided that $k_1 > D_{\max}$ and k_1, $\varepsilon > 0$. Thus, the NSMRL+ITSMS system without NSTESO is Globally Asymptotically Stable (GAS).

B. WITH NSTESO

When NSTESO is deployed, it estimates the unmeasurable disturbance $D(t)$, and actual speed ω_m decreasing the disturbance's impact on the control loop. This section first proves NSTESO stability, then analyzes the combined NSMRL+ITSMS+NSTESO system.

The observer structure is:

$$\begin{cases} \dot{\hat{\omega}} = -\frac{\eta}{J} i_q^* - \frac{B}{J}\omega_m + \hat{D}(t) - a_1 |\tilde{\omega}|^{2/3} \, sign(\tilde{\omega}) \\ \dot{\hat{D}}(t) = -a_2 |\tilde{\omega}|^{1/3} \, sign(\tilde{\omega}) + \hat{d}(t) \\ \dot{\hat{d}}(t) = -a_3 sign(\tilde{\omega}) \end{cases} \tag{48}$$

The disturbance of NSTESO to be replaced by the estimation error:

$$\tilde{D}(t) = \hat{D}(t) - D(t) \tag{49}$$

Consequently, the compensated NSMRL can be expressed as:

$$\dot{s} = -k_1 F(s,t) \tanh(\varepsilon s) - k_2 G(x,t) s + \tilde{D}(t) \tag{50}$$

Lyapunov function includes observer error:

$$L_3 = \frac{1}{2}s^2 + \frac{1}{2}\tilde{\omega}^2 + \frac{1}{2}\tilde{D}^2 + \frac{1}{2}\tilde{d}^2 \tag{51}$$

where $\tilde{\omega} = \hat{\omega} - \omega_m$ and $\tilde{d} = \hat{d} - \dot{D}$.

The time derivative of L_3:

$$\dot{L}_3 = s\dot{s} + \tilde{\omega}\dot{\tilde{\omega}} + \tilde{D}\dot{\tilde{D}} + \tilde{d}\dot{\tilde{d}} = A + A_{obs} \tag{52}$$

First, calculate A:

$$A = s\dot{s} = s\left[-k_1 F(s,t) \tanh(\varepsilon s) - k_2 G(x,t) s + \tilde{D}\right] = \dot{L}_1 + s\tilde{D} \tag{53}$$

Next, calculate A_{obs} (observer Lyapunov derivative, from NSTESO dynamics):

$$A_{obs} = \tilde{\omega}\dot{\tilde{\omega}} + \tilde{D}\dot{\tilde{D}} + \tilde{d}\dot{\tilde{d}} \tag{54}$$

From Eq. (48):

$$\begin{cases} \dot{\tilde{\omega}} = \tilde{D} - a_1 |\tilde{\omega}|^{2/3} \, sign(\tilde{\omega}) \\ \dot{\tilde{D}} = \tilde{d} - a_2 |\tilde{\omega}|^{1/3} \, sign(\tilde{\omega}) \\ \dot{\tilde{d}} = -a_3 sign(\tilde{\omega}) - \ddot{D} \end{cases} \tag{55}$$

Substitute into Eq. (54):

$$A_{obs} = \tilde{\omega}\tilde{D} - a_1 |\tilde{\omega}|^{5/3} + \tilde{D}\tilde{d} - a_2 |\tilde{\omega}|^{4/3} - a_3 |\tilde{\omega}| + \tilde{d}\ddot{D} \tag{56}$$

Thus:

$$\dot{L}_3 = \dot{L}_1 + s\tilde{D} + \tilde{\omega}\tilde{D} - a_1 |\tilde{\omega}|^{5/3} + \tilde{D}\tilde{d} - a_2 |\tilde{\omega}|^{4/3} - a_3 |\tilde{\omega}| + \tilde{d}\ddot{D} \tag{57}$$

To address the coupling terms associated with the disturbance estimation error ($s\tilde{D}$, $\tilde{\omega}\tilde{D}$ and $\tilde{D}\tilde{d}$), Young's inequality is applied to express each product as a weighted sum of squared terms with small tunable coefficients. This treatment ensures that all cross terms remain properly bounded and do not undermine the stabilizing contributions of the control and observer components. With appropriately selected gains (k_1, $k_2 > 0$), $\dot{L}_1 < 0$ the NSMRL control terms dominate the bounded cross terms. In addition, for properly tuned gains (a_1, a_2, $a_3 > 0$), the observer terms ($(-a_1 \mid \tilde{\omega} \mid^{5/3}$ $a_2|\tilde{\omega}|^{4/3} a_3 \mid \tilde{\omega} \mid) - a_1 |\tilde{\omega}|^{5/3} - a_2 |\tilde{\omega}|^{4/3} - a_3 |\tilde{\omega}|$) ensure the NSTESO terms guarantee the decay of the estimation errors.

Consequently, L_3 is positive definite, and its time derivative remains strictly negative for all non-zero states, ensuring the stability of the closed-loop system.

VI. SIMULATION AND EXPERIMENTAL ANALYSIS

To further assess the performance of the novel SMC controller for the SPMSM drive system utilizing NSTESO, both simulations and experiments are performed for the ASMC, MVERL controller, the standard NSMRL based on ITSMS controller, and the NSMRL based on ITSMS controller integrated with the NSTESO.

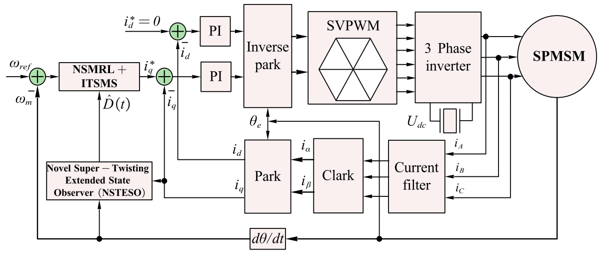

FIGURE 5. Block diagram of SMC model with NSTESO for SPMSM.

The resulting simulation and experimental data are then systematically compared and analyzed. The control architecture of the NSMRL based on ITSMS controller with NSTESO is presented in Fig. 5.

A. SIMULATION RESULTS AND DISCUSSIONS

A simulation model in MATLAB R2019b/Simulink is carried out by integrating the NSMRL+ITSMS control algorithm, based on the NSTESO observer, with the SPMSM. The motor features 5 pole pairs, a permanent magnet flux of 0.0167 Wb, and a rotor inertia of 0.0226 g·m^2. The stator resistance is 0.44 Ω, and the d–q axis inductance is 4.5 mH. The SPMSM is supplied with a DC voltage of 36 V, and the viscous damping is 0.00001 Nms/rad. The inverter switching frequency is set to 10 kHz, with a sampling period of 10 μs.

These parameters are chosen to ensure accurate simulation of the SPMSM drive under the proposed control strategy. The simulation model of the SPMSM drive system employing the NSMRL based on ITSMS controller integrated with NSTESO control strategy is developed in MATLAB 2019R1/Simulink and compared with the ASMC, MVERL and TERL methods, using the parameters listed in Table 1.

In Table 1, an experimental parameter screening procedure was first conducted to identify a feasible and stable parameter

TABLE 1. Gains of the SMC controller for simulation.

Controller	Value		Controller	Value	
PI (current loop)	k_p	1×10^{2}	ASMC	χ	1.2×10^{2}
				k_1	1×10^{-1}
	k_i	4×10^{1}		α	1.5×10^{0}
				β	5×10^{-1}
TERL	k_1	1×10^{-1}	MVERL	k_1	1×10^{-1}
				k_2	1×10^{-1}
	k_2	1×10^{-1}		α	2×10^{0}
				β	5×10^{-1}
	χ	1.2×10^{2}		λ	1.5×10^{-1}
				χ	1.2×10^{2}
NSMRL	k_1	1×10^{-1}	ITSMS	C	2×10^{2}
	k_2	1×10^{-1}		μ	8.5×10^{-1}
	α	2×10^{-1}	NSTESO	a_1	1.5×10^{6}
	β	1.5×10^{-1}			
	ε	2×10^{0}		a_2	1×10^{6}
	σ	1.8×10^{0}		a_3	1×10^{6}

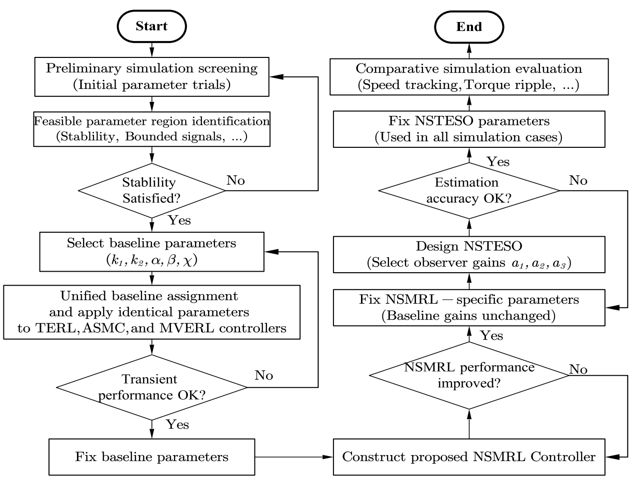

FIGURE 6. Flowchart of the adopted parameter selection strategy ensuring a fair comparison between the proposed NSMRL+ITSMS+NSTESO controller and other SMC schemes.

region for all considered control schemes. This preliminary tuning aims to ensure closed-loop stability and acceptable transient performance under nominal operating conditions. Subsequently, for a fair and meaningful comparison, the main control gains and nonlinear shaping parameters, including k_1, k_2, α, β, and χ, were kept identical for the TERL, ASMC, and MVERL controllers, as these parameters play similar roles in the reaching dynamics and convergence behavior of the respective sliding-mode-based schemes. The adopted parameter selection strategy is further illustrated in Fig. 6.

Based on this unified parameter setting, the proposed NSMRL controller introduces additional nonlinear modulation terms and adaptive reaching components, whose associated parameters are tuned independently without altering the baseline gains shared by the conventional controllers. This strategy ensures that any observed performance improvement—such as faster convergence, reduced torque ripple, or enhanced robustness against load disturbances—can be directly attributed to the newly introduced control structure rather than arbitrary gain amplification.

Moreover, the gains of the proposed NSTESO, namely a_1, a_2, and a_3, are selected following a similar principle. Their values are initially chosen through experimental screening to guarantee fast disturbance estimation without inducing excessive noise sensitivity, and then fixed across all simulation scenarios. This consistent observer configuration further reinforces the fairness of the comparison and highlights the effectiveness of the proposed NSMRL+ ITSMS+NSTESO framework.

1) SPMSM OPERATING UNDER SQUARE-WAVE VARIABLE-SPEED CONDITIONS

Simulation results in Fig.7 under square-wave variable-speed conditions with different load torques (0, 0.02 Nm, and 0.06 Nm) show that NSMRL+NSTESO achieves the fastest tracking of the varying speed, with minimal overshoot, short settling time, and negligible steady-state error across all load conditions.

Fig. 7 compares NSMRL, TERL, ASMC, MVERL, and the proposed NSMRL+NSTESO combination in terms of dynamic and steady-state performance. NSMRL+NSTESO achieves the shortest rise time (about 2 ms), zero overshoot, fast settling, and negligible steady-state error under all load and speed conditions. NSMRL alone exhibits slower response, noticeable overshoot/undershoot, longer settling, and non-negligible steady-state error, particularly under load. TERL, ASMC, and MVERL perform worse, with slower dynamics, larger deviations, and poor robustness. Overall, NSMRL+NSTESO consistently outperforms all other methods across dynamic response, accuracy, and robustness metrics.

TABLE 2. Performance evaluation of speed control methods under varying loads and pulse speeds.

Controller	Convergence speed	Stability	Overshoot	Disturbance rejection
TERL	2	2	2	1
ASMC	2	2	2	2
MVERL	3	3	2	3
NSMRL	4	4	5	4
NSMRL+ NSTESO	**5**	**5**	**4**	**5**

In addition, based on the results shown in Fig. 7, the quality of the proposed methods can be evaluated as follows using a 5-point scale, where the rating increases from low to high values, as described in Table 2. Overall, the integration of NSTESO markedly improves the dynamic performance of

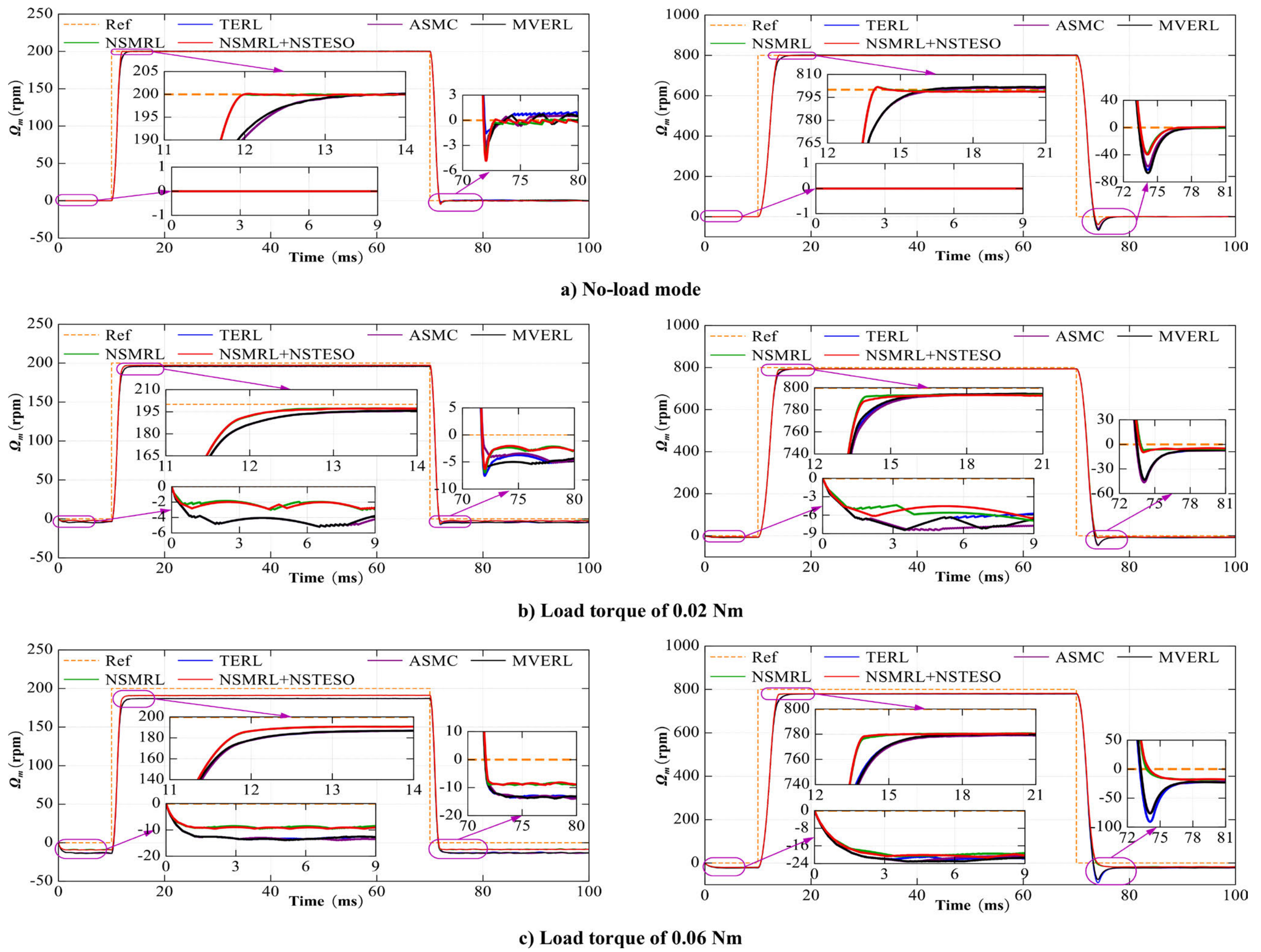

FIGURE 7. Simulation results of the motor under square-wave speed variation with different load values.

TABLE 3. Performance evaluation of speed control methods under varying speeds and pulse torques.

Controller	Convergence speed	Stability	Overshoot	Disturbance rejection
TERL	2	2	2	2
ASMC	2	2	2	2
MVERL	3	1	2	3
NSMRL	4	4	4	4
NSMRL+ NSTESO	**5**	**5**	**5**	**5**

the NSMRL controller, making NSMRL+NSTESO the most effective method among those evaluated.

2) SPMSM IN STARTUP MODE UNDER VARYING LOAD CONDITIONS

This section evaluates the system under torque pulses of 0.02 Nm and 0.06 Nm at speeds of 300 rpm and 1000 rpm, as illustrated in Fig. 8.

In Fig. 8, NSMRL+NSTESO responds rapidly to torque pulses, maintaining precise speed with minimal fluctuations. In contrast, NSMRL alone shows slower recovery and minor deviations, while TERL, ASMC, and MVERL exhibit prolonged transients and pronounced overshoot or undershoot. These results demonstrate the proposed method's superior disturbance rejection and robust high-speed tracking under dynamic torque variations.

Furthermore, the results presented in Fig. 8 allow a comparative evaluation of the proposed methods using a five-point performance scale, where higher scores indicate better performance, as summarized in Table 3.

3) SPMSM UNDER TRAPEZOIDAL VARIABLE-SPEED OPERATION

Fig. 9 compares the proposed NSMRL+NSTESO with NSMRL, TERL, ASMC, and MVERL under trapezoidal speed profiles (400 rpm/1000 rpm, no-load/0.06 Nm load). NSMRL+NSTESO achieves the fastest rise (around 30 ms), zero overshoot, precise profile tracking, and immediate

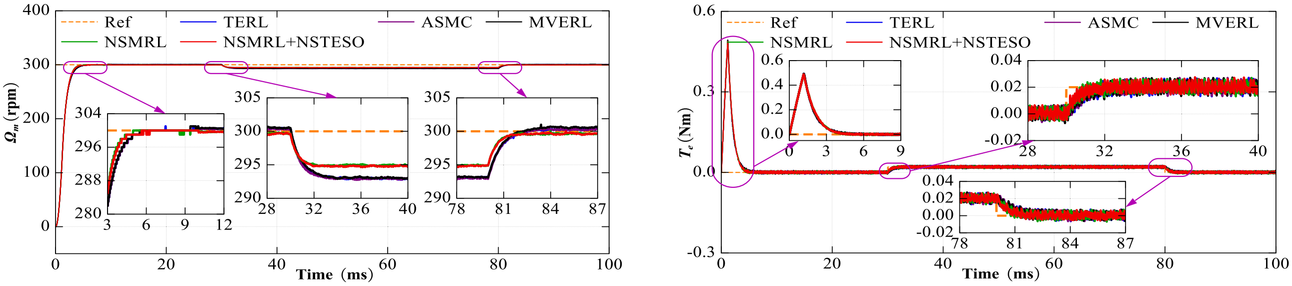

a) 300 rpm with 0.02 Nm square-wave torque

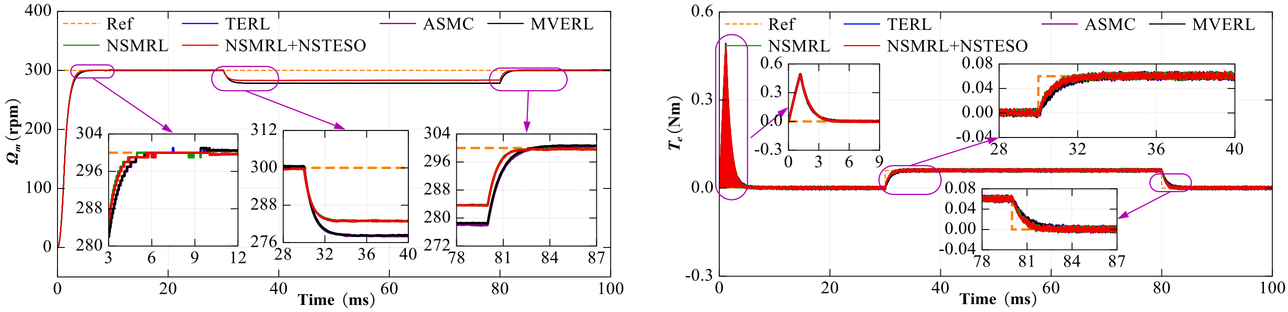

b) 300 rpm with 0.06 Nm square-wave torque

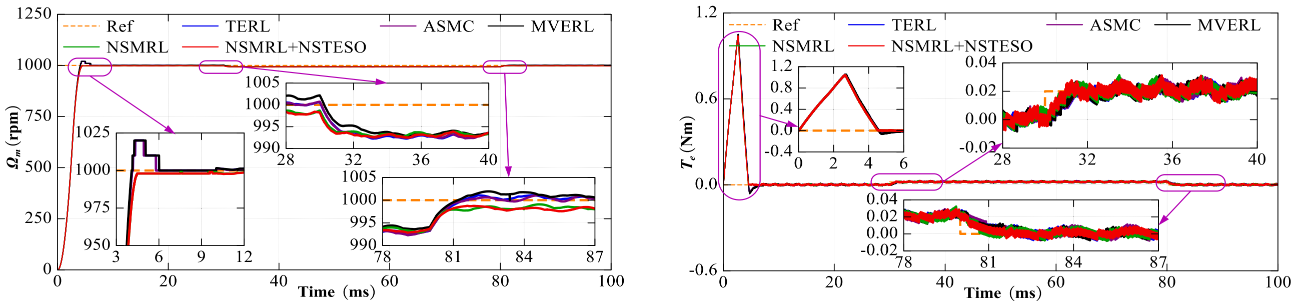

c) 1000 rpm with 0.02 Nm square-wave torque

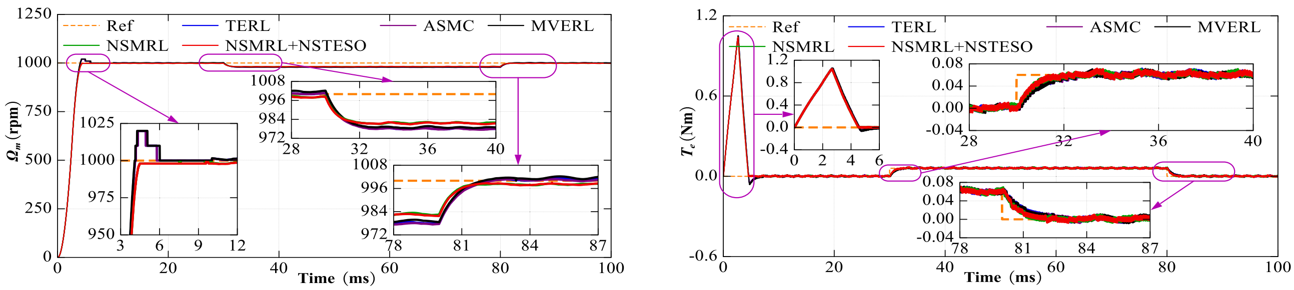

d) 1000 rpm with 0.06 Nm square-wave torque

FIGURE 8. Simulation results of the motor under square-wave torque variations at different speed values.

settling in all scenarios. NSMRL alone shows slower rise and minor-to-moderate overshoot/undershoot, while TERL, ASMC, and MVERL exhibit the slowest response, large deviations, and prolonged settling. Under load (Fig. 9b and Fig. 9d), NSMRL+NSTESO maintains robust torque disturbance rejection with negligible residual error. Overall, NSMRL+NSTESO consistently outperforms alternatives in rise time, overshoot, settling, and load resilience.

These results indicate that the NSMRL+NSTESO and NSMRL exhibit robust disturbance rejection and adaptive capabilities, making them the most effective methods for precise speed control in trapezoidal motion scenarios.

Overall, the best balance of dynamic response, steady-state precision, and load disturbance resilience is demonstrated by the NSMRL+NSTESO and NSMRL across all tested speed levels and load conditions.

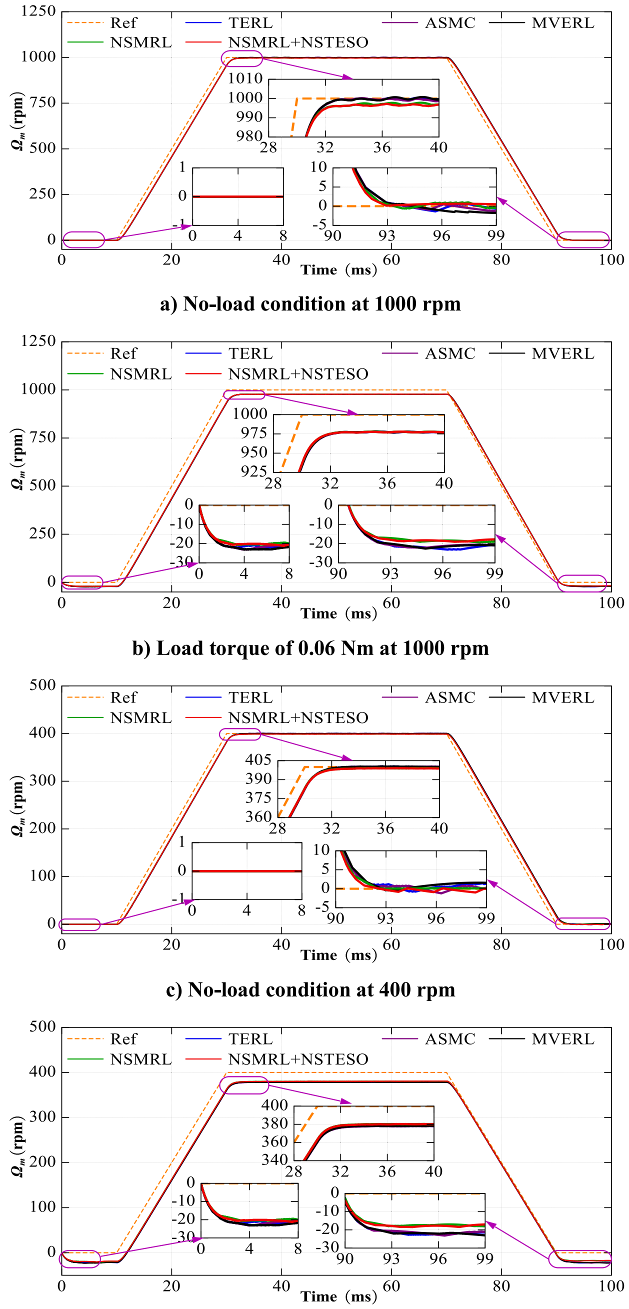

a) No-load condition at 1000 rpm

b) Load torque of 0.06 Nm at 1000 rpm

c) No-load condition at 400 rpm

d) Load torque of 0.06 Nm at 400 rpm

FIGURE 9. Simulation results of SPMSM speed under trapezoidal speed profiles for no-load and 0.06 Nm load conditions.

B. EXPERIMENTAL RESULTS AND DISCUSSIONS

The experimental validation is performed using a physical SPMSM drive system controlled by a TMS320F28335 DSP (Texas Instruments), as illustrated in Fig. 10. The motor employed shares the same specifications as in the simulation: five pole pairs, a permanent magnet flux of 0.0167 Wb, rotor inertia of 0.0226 g·m^2, stator resistance of 0.44 Ω, and d–q axis inductances of 4.5 mH. The SPMSM is powered by a 36 V DC bus, with viscous damping of 0.00001 Nms/rad.

TABLE 4. Gains of the SMC controller and NSTESO for experimental motor drive system.

Controller	Value		Controller	Value	
PI (Current loop)	k_p	6×10^{-1}	ASMC	χ	1×10^{4}
				k_1	1×10^{5}
	k_i	1×10^{-4}		α	2×10^{0}
				β	5×10^{-1}
TERL	k_1	1×10^{2}	MVERL	k_1	1×10^{2}
				k_2	5×10^{2}
	k_2	5×10^{2}		α	2×10^{0}
				β	5×10^{-1}
	χ	1×10^{4}		λ	1.5×10^{0}
				χ	2×10^{5}
NSMRL	k_1	1×10^{2}	ITSMS	C	1×10^{5}
	k_2	5×10^{2}		μ	1×10^{0}
	α	2×10^{0}	NSTESO	a_1	1×10^{5}
	β	5×10^{-1}			
	ε	2×10^{0}		a_2	1×10^{0}
	σ	4×10^{0}		a_3	1×10^{0}

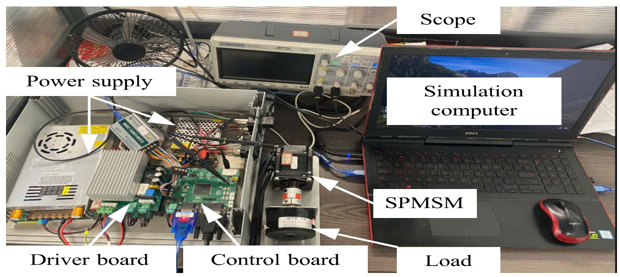

FIGURE 10. Experimental platform of SPMSM drive system.

The three-phase inverter switches at 10 kHz, and the control system runs at a 100 μs sampling period, consistent with the simulation configuration.

In the experimental implementation, the control parameters of the four controllers are tuned using the procedure illustrated in Fig. 6, and the resulting controller and observer parameter values are reported in Table 4.

1) SPEED RESPONSE ANALYSIS OF SPMSM IN NO-LOAD MODE

To verify the dynamic response of the proposed scheme, experimental results of the motor's speed response during the no-load starting process are presented for reference speeds of 450 rpm, 900 rpm and 1200 rpm. The comparative results of five control schemes (TERL, ASMC, MVERL, NSMRL, and proposed NSMRL+NSTESO) are shown in Fig. 11.

Based on the experimental results shown in Fig. 11 and Table 5 at the three tested speeds, NSMRL and NSMRL+NSTESO consistently achieve lower overshoot and faster convergence compared with the other methods. At 450 rpm,

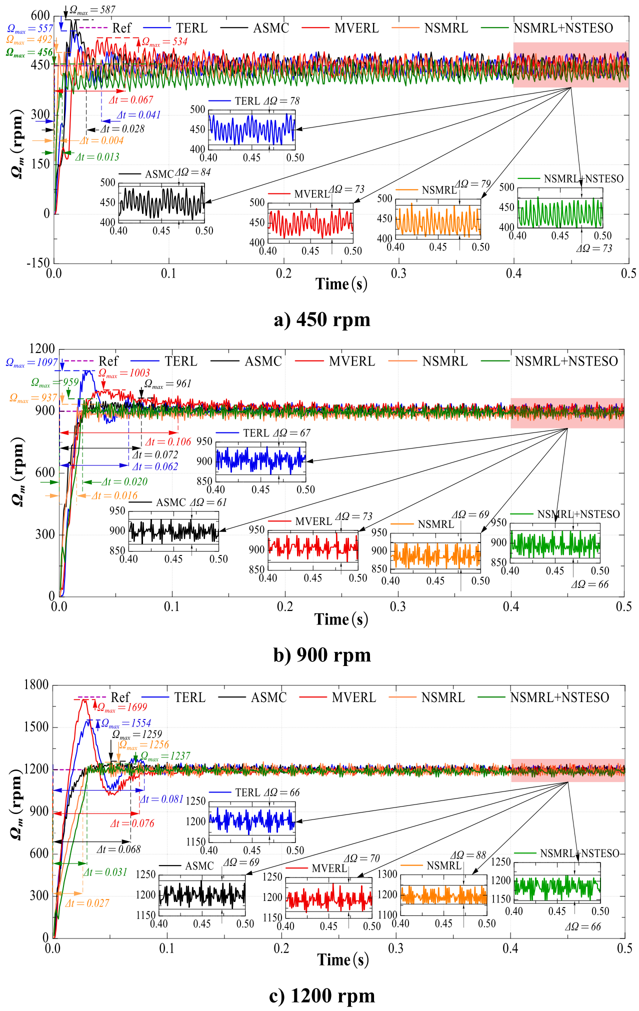

FIGURE 11. Experimental results of SPMSM speed under no-load condition with different starting speeds.

NSMRL reaches a convergence time of only 4 ms, while NSMRL+NSTESO exhibits the lowest overshoot (456 rpm).

As the speed increases to 900 rpm and 1200 rpm, both methods continue to maintain minimal speed deviations and rapid tracking capabilities, demonstrating strong stability across a wide speed range.

In contrast, TERL and MVERL generally produce the highest overshoot and the longest convergence times, particularly at higher speeds. ASMC shows improved convergence performance but still suffers from relatively large overshoot.

The SPMSM starts under no-load conditions at 750 rpm. As shown in Fig. 12a, when the speed is increased from 750 rpm to 900 rpm, the TERL method produces the largest overshoot, reaching 972 rpm, and requires 40 ms to return to steady state. The ASMC method reaches 942 rpm and exhibits a slow recovery time of 88 ms, indicating limited dynamic responsiveness. The MVERL method shows moderate behavior, with an overshoot of 948 rpm and a recovery time of 47 ms. The NSMRL method demonstrates a very fast transient response, reaching 947 rpm and recovering

TABLE 5. Comparative analysis of experimental results at different speeds in no-load conditions.

Speed (rpm)	Controller	Overshoot index (rpm)	Speed deviation $\Delta\Omega$ (rpm)	Convergence time (ms)
450	TERL	557	78	41
	ASMC	587	84	28
	MVERL	534	73	67
	NSMRL	492	79	4
	NSMRL+ NSTESO	**456**	**73**	**13**
900	TERL	1097	67	62
	ASMC	961	61	72
	MVERL	1003	73	106
	NSMRL	933	69	16
	NSMRL+ NSTESO	**952**	**66**	**20**
1200	TERL	1554	66	81
	ASMC	1259	69	68
	MVERL	1699	70	76
	NSMRL	1270	88	27
	NSMRL+ NSTESO	**1237**	**66**	**31**

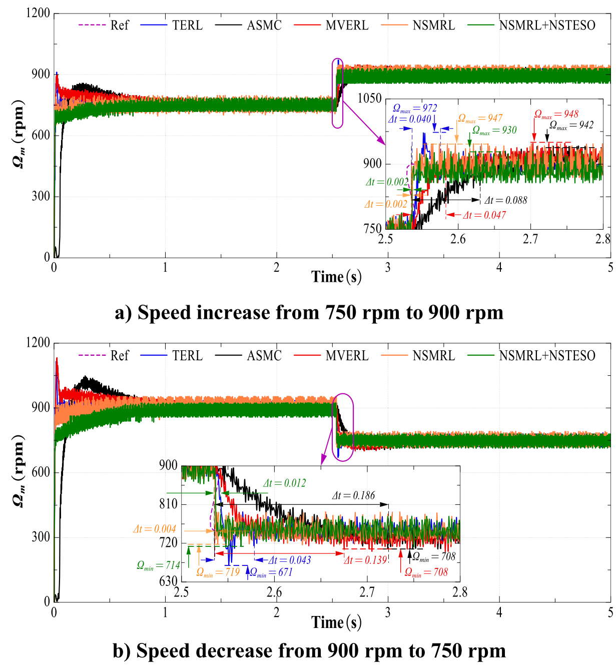

FIGURE 12. Experimental SPMSM speed performance under no-load with variable speed conditions.

in only 2 ms. The NSMRL combined with the nonlinear extended state observer achieves the smallest overshoot of 930 rpm and maintains a fast recovery time of 2 ms, resulting in the best acceleration-phase performance.

According to Fig. 12b, when the speed suddenly decreases from 900 rpm to 750 rpm, the TERL method produces the

TABLE 6. Comparison of experimentally achieved parameters at different speeds with no-load mode.

Controller	Overshoot index	Speed deviation	Convergence time	Dynamic speed transition
TERL	1	4	3	1
ASMC	3	3	1	2
MVERL	2	2	2	3
NSMRL	4	1	5	4
Proposed NSMRL+ NSTESO	**5**	**5**	**4**	**5**

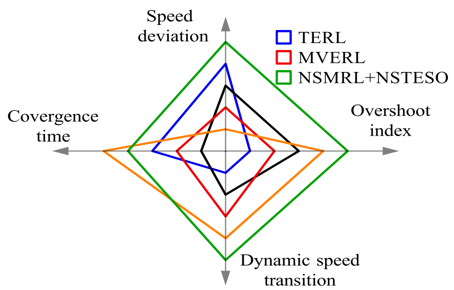

FIGURE 13. Performance evaluation of NSMRL+NSTESO compared with other SMC methods under no-load conditions.

largest undershoot, dropping to 671 rpm, with a recovery time of 43 ms. The ASMC method decreases to 708 rpm and exhibits the slowest recovery time of 186 ms. The MVERL method also reaches 708 rpm but recovers in 139 ms, indicating moderate stability. The NSMRL method demonstrates strong dynamic performance, with an undershoot of 719 rpm and a rapid recovery time of 4 ms. The NSMRL combined with the nonlinear extended state observer achieves the smallest undershoot of 714 rpm and recovers in 12 ms, representing the best overall deceleration performance with minimal deviation.

Based on the above no-load cases, an evaluation table of the control method parameters using a 5-point scoring system is presented in Table 6.

Based on Fig. 13, the proposed NSMRL+NSTESO method, represented by the green area, covers the largest portion of the radar plot compared with TERL (blue), ASMC (black), and MVERL (orange), indicating superior overall performance under no-load conditions. The expanded green area reflects minimal overshoot, high speed-tracking accuracy, fast convergence, and effective handling of dynamic speed transitions. This confirms that integrating NSMRL with the nonlinear extended state observer significantly enhances dynamic response and robustness.

2) SPMSM IN STARTUP MODE UNDER LOAD CONDITIONS

To further validate the dynamic performance of the proposed approach, experimental speed responses during load-start conditions are provided for reference speeds of 450 rpm, 900 rpm, and 1200 rpm. The corresponding comparisons

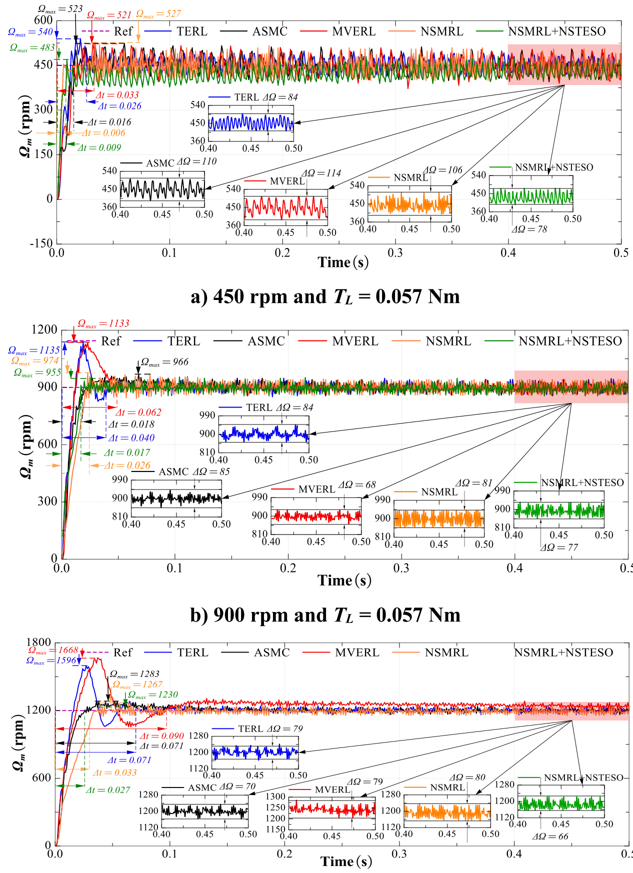

a) 450 rpm and T_L = 0.057 Nm

b) 900 rpm and T_L = 0.057 Nm

c) 1200 rpm and T_L = 0.057 Nm

FIGURE 14. Experimental results of SPMSM speed under various initial speeds and load conditions.

among the five control strategies (TERL, ASMC, MVERL, NSMRL, and NSMRL+NSTESO) are illustrated in Fig. 14.

From the load-startup results in Fig. 14 and Table 7, the NSMRL+NSTESO method exhibits the smallest overshoot at all speeds, reaching only 483 rpm at 450 rpm, 955 rpm at 900 rpm, and 1230 rpm at 1200 rpm, which is significantly lower than TERL, whose overshoot peaks at 540 rpm, 1135 rpm, and 1596 rpm, respectively. The steady-state speed deviation is also minimized, with NSMRL+NSTESO maintaining fluctuations of 78 rpm at 450 rpm, 77 rpm at 900 rpm, and 66 rpm at 1200 rpm, outperforming ASMC, NSMRL, and TERL across most cases. In terms of convergence time, NSMRL+NSTESO stabilizes within 9 ms at 450 rpm, 18 ms at 900 rpm, and 27 ms at 1200 rpm, much faster than MVERL, which requires up to 90 ms at higher speeds. Although ASMC achieves fast convergence in some cases, its deviation and overshoot remain larger.

Overall, the combined NSMRL+NSTESO method demonstrates the most balanced performance, achieving low overshoot, small speed deviation, and short stabilization time across all load-startup scenarios.

The dynamic evaluation in Fig. 15 under load conditions shows that during the speed increase from 300 rpm

TABLE 7. Comparative analysis of experimental results at different speeds in load conditions.

Speed (rpm)	Controller	Overshoot index (rpm)	Speed deviation $\Delta\Omega$ (rpm)	Convergence time (ms)
450	TERL	540	84	26
	ASMC	523	110	16
	MVERL	521	114	33
	NSMRL	527	106	6
	NSMRL+ NSTESO	**483**	**78**	**9**
900	TERL	1135	84	40
	ASMC	966	85	18
	MVERL	1133	68	62
	NSMRL	974	81	26
	NSMRL+ NSTESO	**955**	**77**	**18**
1200	TERL	1596	79	71
	ASMC	1283	70	71
	MVERL	1668	79	90
	NSMRL	1267	80	33
	NSMRL+ NSTESO	**1230**	**66**	**27**

TABLE 8. Comparison of experimentally achieved parameters at different speeds with load mode.

Controller	Overshoot index	Speed deviation	Convergence time	Dynamic speed transition
TERL	1	4	3	1
ASMC	3	3	2	2
MVERL	2	1	1	3
NSMRL	4	2	5	4
NSMRL+ NSTESO	**5**	**5**	**4**	**5**

to 600 rpm, the NSMRL+NSTESO achieves the lowest overshoot at 630 rpm, while TERL exhibits the largest overshoot at 714 rpm. In terms of recovery, NSMRL reaches steady state with the fastest at 5 ms, followed by the NSMRL+NSTESO at 8 ms, whereas ASMC suffers from a severe delay of 779 ms.

For the speed decrease from 600 to 300 rpm, TERL yields the smallest undershoot at 167 rpm, while NSMRL+ NSTESO records the highest at 263 rpm but still maintains a short recovery time of 30 ms, second only to TERL at 24 ms. ASMC again shows poor responsiveness with a 575 ms recovery time. Overall, NSMRL provides the best performance for speed increases, whereas NSMRL+ NSTESO delivers the most balanced behavior across both acceleration and deceleration. TERL recovers quickly but exhibits large transient deviations, and MVERL remains moderate. In contrast, ASMC consistently demonstrates the slowest recovery, making it unsuitable for rapid speed transitions.

From the analyzed load cases, Table 8 provides a 5-point performance assessment of the control method parameters.

Based on Fig. 16, the proposed NSMRL+NSTESO method, represented by the green area, covers the largest portion of the radar plot compared with TERL (blue), ASMC

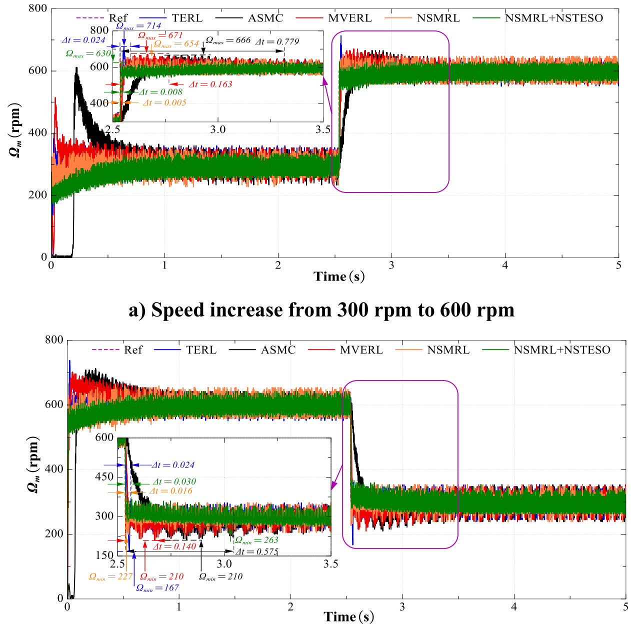

a) Speed increase from 300 rpm to 600 rpm

b) Speed decrease from 600 rpm to 300 rpm

FIGURE 15. Experimental results of SPMSM speed under various load and variable speed conditions.

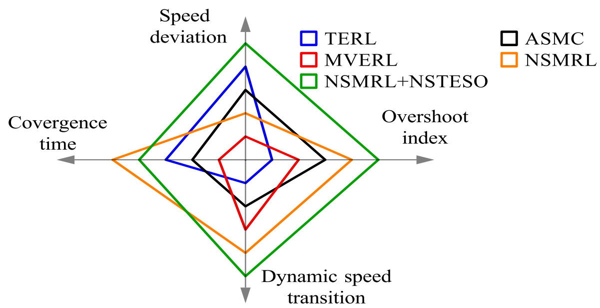

FIGURE 16. Comparative performance of the NSMRL+NSTESO scheme and other SMC controllers under load conditions.

(black), NSMRL (orange), and MVERL (red), indicating superior overall performance under load conditions. The expanded green area reflects minimal overshoot index, small speed deviation, fast convergence time, and effective handling of dynamic speed transitions. This confirms that integrating NSMRL with the nonlinear extended state observer significantly enhances dynamic response and robustness under load. In contrast, TERL shows notable overshoot and speed deviation, ASMC has relatively large convergence time and overshoot, MVERL exhibits moderate performance in some metrics but lacks comprehensiveness, while NSMRL, though better than TERL and ASMC in parts, still does not match NSMRL+NSTESO in overall performance.

3) SPMSM UNDER TRAPEZOIDAL VARIABLE-SPEED OPERATION

This section presents a detailed analysis of the speed and q-axis current responses for multiple control strategies,

TABLE 9. Comparative analysis of experimental results under trapezoidal variable-speed profiles at different load conditions.

Load (Nm)	Controller	Overshoot index (rpm)	Speed deviation $\Delta\Omega_{max}$ (rpm)	I_{qmax} current (A)
No-load	TERL	942	306	0.208
	ASMC	977	307	0.159
	MVERL	978	492	0.541
	NSMRL	977	138	0.386
	NSMRL+ NSTESO	**942**	**103**	**0.184**
0.054	TERL	960	365	0.213
	ASMC	996	396	0.190
	MVERL	972	305	0.185
	NSMRL	972	144	0.558
	NSMRL+ NSTESO	**942**	**108**	**0.213**
0.084	TERL	948	443	0.360
	ASMC	996	360	0.188
	MVERL	990	359	0.385
	NSMRL	974	140	0.557
	NSMRL+ NSTESO	**954**	**127**	**0.274**
0.111	TERL	960	438	0.322
	ASMC	1002	276	0.202
	MVERL	984	383	0.304
	NSMRL	966	136	0.502
	NSMRL+ NSTESO	**960**	**126**	**0.330**

including TERL, ASMC, MVERL, NSMRL, and NSMRL+NSTESO, under varying load conditions. The evaluation is performed using a complex trapezoidal reference speed profile to assess the transient and steady-state performance of each method.

The experimental evaluation under trapezoidal variable-speed profiles and four load levels (0 Nm to 0.111 Nm) in Fig. 17 and Table 9 shows that the proposed NSMRL+NSTESO consistently provides the best speed stability, achieving the lowest speed deviation of 103 rpm to 127 rpm, whereas the worst-performing methods (MVERL or TERL depending on the load) reach 438 rpm to 492 rpm. Overshoot control is also enhanced, with the NSMRL+NSTESO maintaining 942 rpm to 960 rpm, compared with the highest overshoot values of 996 rpm to 1002 rpm observed in ASMC. Regarding current performance, ASMC achieves the lowest I_q $I_{q,max}$(0.159 A to 0.202 A), while NSMRL and MVERL produce the highest values (0.502 A to 0.558 A). The NSMRL+NSTESO maintains a balanced current range of 0.184 A to 0.330 A, providing better efficiency than NSMRL while achieving superior speed accuracy. Overall, the proposed NSMRL+NSTESO method offers the most robust combination of low overshoot, minimal speed deviation, and acceptable current consumption, making it the most effective controller for precise variable-speed operation across all load conditions.

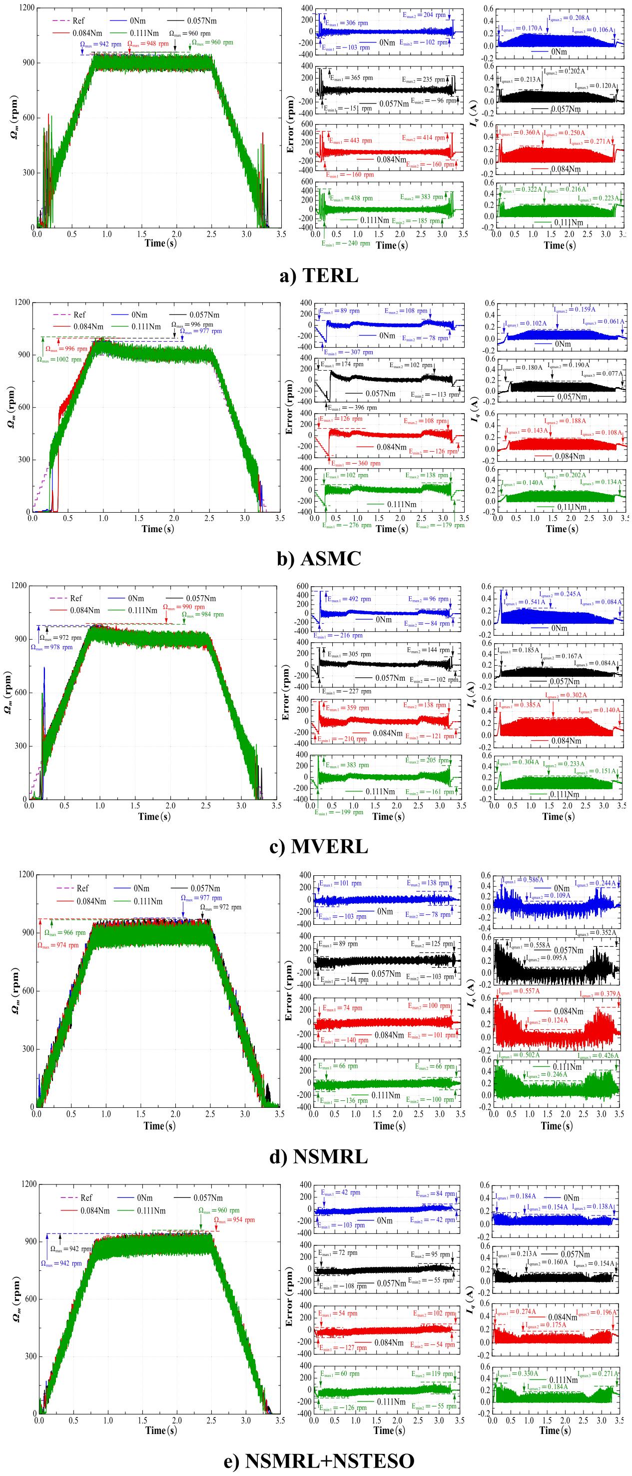

FIGURE 17. Experimental results of SPMSM speed under a trapezoidal speed input with different load conditions.

From the analyzed trapezoidal variable-speed profiles at four load levels, Table 10 presents a five-point performance assessment of the control method parameters.

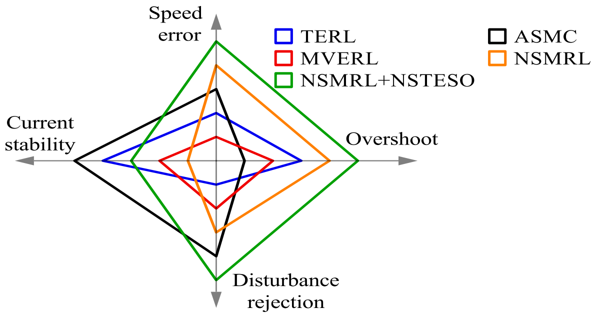

FIGURE 18. Comparative performance of NSMRL+NSTESO and SMC methods under trapezoidal speed profiles with varying loads.

TABLE 10. Performance evaluation of speed control methods under trapezoidal variable-speed profiles at four load levels.

Controller	Overshoot	Speed error	Current stability	Disturbance rejection
TERL	3	2	4	1
ASMC	1	3	5	4
MVERL	2	1	2	2
NSMRL	4	4	1	3
NSMRL+ NSTESO	**5**	**5**	**3**	**5**

The radar chart evaluation highlights the advantages of the proposed NSMRL+NSTESO method across four parameters (Fig. 18 and Table 10): speed error, overshoot, disturbance rejection, and current stability. The NSMRL + NSTESO (green line) covers the largest area, demonstrating superior and balanced performance, particularly in speed error and disturbance rejection, while maintaining solid overshoot and current stability. TERL (blue line) shows moderate coverage with decent performance but falls short in speed error and disturbance rejection. MVERL (red line) exhibits the smallest area, indicating weaknesses across most parameters. ASMC (black line) excels in current stability but is limited by poorer speed error and overshoot. NSMRL (orange line) shows notable gaps, confirming that the integration of NSTESO significantly enhances overall performance.

4) SPEED RESPONSE FOR DIFFERENT COEFFICIENTS OF HYPERBOLIC TANGENT FUNCTION IN PROPOSED NSMRL METHOD

This section proceeds by comparing and identifying the optimized ε parameters of the hyperbolic tangent and sign functions, while keeping all other system parameters unchanged, as listed in Table 4. It also presents an experimental comparison of start-up speed performance under a load condition of $T_L = 0.057$ Nm in SPMSM drive systems employing the NSMRL+NSTESO control strategy.

Experimental results for different ε coefficient cases are presented in Fig. 19 and Table 11.

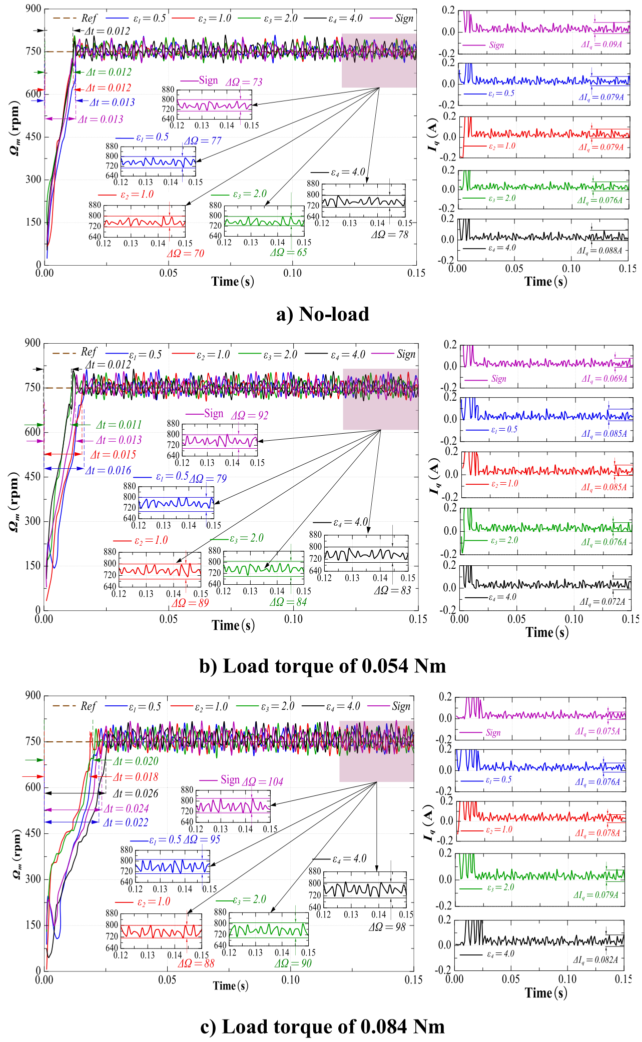

FIGURE 19. Speed and q-axis current responses under different ε parameters of hyperbolic tangent and sign functions in proposed NSMRL +NSTESO strategy with different load conditions.

Based on Table 11 and the corresponding figures, the ε-coefficients of the Tanh function were evaluated using convergence time, maximum speed deviation, and q-axis current fluctuation under three load conditions. Across all cases, the coefficients $\varepsilon = 1.0$ and $\varepsilon = 2.0$ consistently outperform the conventional Sign function, offering faster convergence and smaller dynamic errors. The coefficient $\varepsilon = 1.0$ provides the best overall balance between convergence speed and speed deviation, while $\varepsilon = 2.0$ achieves the lowest current fluctuation and superior response under load. Considering all criteria, $\varepsilon = 2.0$ yields the most robust and well-rounded performance for the sliding-mode control surface.

5) SPEED RESPONSE UNDER CHANGES IN SPMSM PARAMETERS

In this paper, the speed control framework is further refined by omitting the influence of stator inductance and resistance in the design stage. Instead, the emphasis is placed on

TABLE 11. Experimental results comparison for different parameters of hyperbolic tangent and sign functions.

Load (Nm)	Coefficient	Convergence time (ms)	Speed deviation $\Delta\Omega_{max}$ (rpm)	ΔI_q (A)
No-load	Sign	13	73	0.090
	$\varepsilon_1 = 0.5$	13	77	0.079
	$\varepsilon_2 = 1.0$	12	70	0.079
	$\varepsilon_3 = 2.0$	**12**	**65**	**0.076**
	$\varepsilon_4 = 4.0$	12	78	0.088
0.054	Sign	13	92	0.069
	$\varepsilon_1 = 0.5$	16	79	0.085
	$\varepsilon_2 = 1.0$	15	89	0.085
	$\varepsilon_3 = 2.0$	**11**	**84**	**0.076**
	$\varepsilon_4 = 4.0$	12	83	0.072
0.084	Sign	24	104	0.075
	$\varepsilon_1 = 0.5$	22	95	0.076
	$\varepsilon_2 = 1.0$	18	88	0.078
	$\varepsilon_3 = 2.0$	**20**	**90**	**0.079**
	$\varepsilon_4 = 4.0$	26	98	0.082

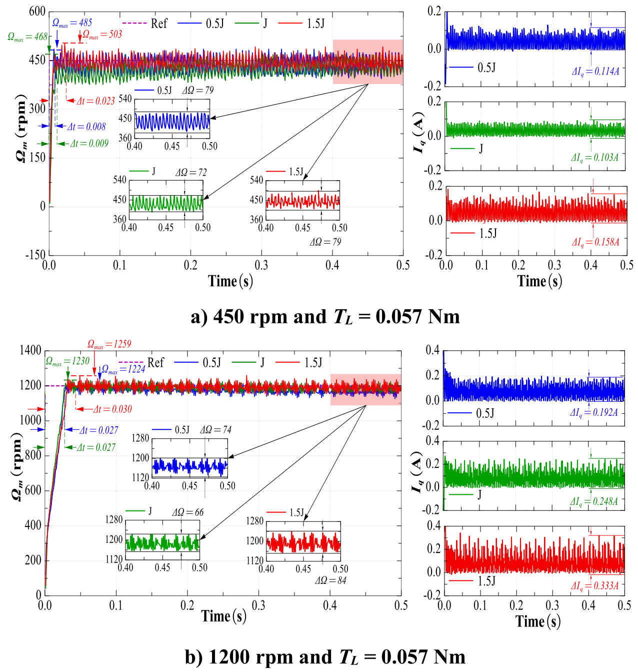

FIGURE 20. Speed response under different inertia mismatches at multiple rated speeds under a 0.057 Nm load.

strengthening the robustness of the SPMSM speed regulation scheme when the system operates under inertia mismatch conditions. This approach allows the controller to better maintain dynamic performance despite uncertainties in the mechanical parameters.

At various speeds with a load of 0.057 Nm, the speed responses of the NSMRL+NSTESO are presented in Fig. 20 for different inertia mismatches.

In Fig. 20, the impact of inertia variation on the NSMRL +NSTESO scheme is assessed using convergence time, overshoot, maximum speed deviation, and q-axis current fluctuation at 450 rpm and 1200 rpm under a 0.057 Nm load. The results show that increasing inertia (e.g., 1.5J) consistently leads to slower convergence, larger overshoot, and higher current fluctuation, indicating degraded dynamic performance. Reducing inertia (0.5J) improves convergence speed but tends to increase overshoot. Under both speed conditions, the nominal inertia J provides the smallest speed deviation and, at 450 rpm, the lowest overshoot and current ripple, demonstrating that the controller is tuned for the nominal mechanical parameters. Although the method maintains acceptable performance under inertia mismatches, higher speeds exacerbate dynamic degradation across all cases.

Overall, the nominal inertia offers the best balance, while significant inertia deviations negatively affect transient behavior and current stability.

Table 12 compares the performance of existing related control methods (e.g., TERL, ASMC, and MVERL) with the proposed NSMRL+NSTESO scheme across key parameters. The NSMRL+NSTESO consistently demonstrates superior performance, achieving low steady-state deviation, minimal speed overshoot, fast settling time, reduced chattering, high disturbance rejection capability, excellent dynamic response quality, and the highest control efficiency. TERL and MVERL show moderate overall performance but suffer from high overshoot and chattering, while ASMC exhibits high steady-state deviation, slow settling time, and lower dynamic response quality despite moderate overshoot.

TABLE 12. Comparative performance of proposed NSMRL+NSTESO scheme and existing control methods.

Controller	TERL	ASMC	MVERL	Proposed NSMRL+ NSTESO
Steady-state deviation	Moderate	High	High	**Low**
Spead overshoot	High	Moderate	High	**Low**
Speed settling time	Moderate	High	High	**Low**
Chattering analysis	High	Moderate	High	**Low**
Disturbance rejection capability	Moderate	Low	Moderate	**High**
Dynamic response quality	Moderate	Low	Moderate	**High**
Control efficiency	Moderate	Good	Good	**Excellent**

Overall, the table confirms that the integration of NSMRL with the nonlinear extended state observer provides the most balanced and robust control solution, outperforming conventional methods in accuracy, stability, and efficiency.

VII. CONCLUSION

This research proposed a comprehensive robust speed control framework for SPMSM drives by suitably integrating the NSMRL law, ITSMS surface, and NSTESO observer to substantially improve the stability and performance of SPMSM drive control systems. The uniquely integrated design addresses the key challenges in high-performance motor control effectively, including chattering, parameter uncertainties, unmodeled dynamics, and time-varying external disturbances. The NSMRL significantly reduces switching oscillations while preserving the robustness of sliding-mode control. Meanwhile, the ITSMS ensures finite-time convergence and eliminates steady-state error, and the NSTESO provides accurate real-time disturbance estimation with guaranteed GAS through Lyapunov analysis.

Extensive simulations and real-time experiments using the TMS320F28335 digital signal processor confirmed that the proposed controller consistently outperforms the existing TERL, ASMC, and MVERL methods in terms of overshoot suppression, dynamic response, disturbance rejection, and regulation of motor current. The analytical and experimental results also demonstrated that the introduced NSMRL+ NSTESO structure with the ITSMS offers a greatly practical, efficient, and reliable solution suitable for industrial servo systems requiring high robustness and smooth control action under various operating conditions and disturbances.

Future research will focus on extending the proposed method to multi-axis PMSM platforms and nonlinear electromechanical systems with stronger coupling effects. Additionally, adaptive or learning-based mechanisms will be explored to automatically tune the controller and observer gains under varying operating conditions. The applications of the introduced framework to high-speed, low-inductance motors and energy-efficient electric drive systems will also be investigated to further enhance industrial applicability.

REFERENCES

[1] S.-G. Lee, S. Kim, J.-C. Park, M.-R. Park, T. H. Lee, and M.-S. Lim, "Robust design optimization of SPMSM for robotic actuator considering assembly imperfection of segmented stator core," *IEEE Trans. Energy Convers.*, vol. 35, no. 4, pp. 2076–2085, Dec. 2020.

[2] R. Sreejith and B. Singh, "Sensorless predictive control of SPMSM-driven light EV drive using modified speed adaptive super twisting sliding mode observer with MAF-PLL," *IEEE J. Emerg. Sel. Topics Ind. Electron.*, vol. 2, no. 1, pp. 42–52, Jan. 2021.

[3] J. Lara, J. Xu, and A. Chandra, "Effects of rotor position error in the performance of field-oriented-controlled PMSM drives for electric vehicle traction applications," *IEEE Trans. Ind. Electron.*, vol. 63, no. 8, pp. 4738–4751, Aug. 2016.

[4] L. He, F. Wang, W. Tian, J. Rodríguez, and M. L. Heldwein, "Predefined-time sliding mode predictive current control for disturbance suppression and dynamic response improvement in SPMSM drives," *IEEE Trans. Ind. Electron.*, vol. 72, no. 2, pp. 1292–1302, Feb. 2025.

[5] A. T. Nguyen, B. A. Basit, H. H. Choi, and J.-W. Jung, "Disturbance attenuation for surface-mounted PMSM drives using nonlinear disturbance observer-based sliding mode control," *IEEE Access*, vol. 8, pp. 86345–86356, 2020.

[6] R. Errouissi, M. Ouhrouche, W.-H. Chen, and A. M. Trzynadlowski, "Robust cascaded nonlinear predictive control of a permanent magnet synchronous motor with antiwindup compensator," *IEEE Trans. Ind. Electron.*, vol. 59, no. 8, pp. 3078–3088, Aug. 2012.

[7] J. Liu, H. Li, and Y. Deng, "Torque ripple minimization of PMSM based on robust ILC via adaptive sliding mode control," *IEEE Trans. Power Electron.*, vol. 33, no. 4, pp. 3655–3671, Apr. 2018.

[8] S. Ye and X. Yao, "An enhanced SMO-based permanent-magnet synchronous machine sensorless drive scheme with current measurement error compensation," *IEEE J. Emerg. Sel. Topics Power Electron.*, vol. 9, no. 4, pp. 4407–4419, Aug. 2021.

[9] T. T. Tuyen, J. Yang, L. Liao, and J. Zhou, "Integrated sliding mode control for permanent magnet synchronous motor drives based on second-order disturbance observer and low-pass filter," *Electronics*, vol. 14, no. 7, pp. 1–25, Apr. 2025.

[10] M. S. Zaky, "A self-tuning PI controller for the speed control of electrical motor drives," *Electric Power Syst. Res.*, vol. 119, pp. 293–303, Feb. 2015.

[11] A. Brosch, O. Wallscheid, and J. Böcker, "Time-optimal model predictive control of permanent magnet synchronous motors considering current and torque constraints," *IEEE Trans. Power Electron.*, vol. 38, no. 7, pp. 7945–7957, Jul. 2023.

[12] Y. Wang, Y. Feng, X. Zhang, and J. Liang, "A new reaching law for antidisturbance sliding-mode control of PMSM speed regulation system," *IEEE Trans. Power Electron.*, vol. 35, no. 4, pp. 4117–4126, Apr. 2020.

[13] Y. Zhang, Q.-G. Wang, J. Liu, and J. Yu, "Command filtered fuzzy adaptive control for PMSMs with time-varying state constraints and stochastic disturbances," *IEEE Trans. Transport. Electrific.*, vol. 10, no. 3, pp. 5614–5623, Sep. 2024.

[14] T. T. Tuyen, J. Yang, L. Liao, and N. G. M. Thao, "Recent advances in sliding mode control techniques for permanent magnet synchronous motor drives," *Electronics*, vol. 14, no. 19, p. 3933, Oct. 2025.

[15] H. N. Tran and J. W. Jeon, "Robust speed controller using dual adaptive sliding mode control (DA-SMC) method for PMSM drives," *IEEE Access*, vol. 11, pp. 63261–63270, 2023.

[16] T. Ur Rahman, A. Ullah, S. Ullah, J. Pan, B. Alghamdi, A. Rehman, and Z. Ouyang, "Fast smooth super-twisting SMC and super-twisting disturbance estimation for PMSM speed control," *IEEE Trans. Consum. Electron.*, vol. 71, no. 4, pp. 10160–10171, Nov. 2025.

[17] A. B. Alhassan, M. A. Shehu, V. Gali, and T. D. Do, "Disturbance observer-based super-twisting SMC for variable speed wind energy conversion system under parametric uncertainties," *IEEE Access*, vol. 13, pp. 11003–11020, 2025.

[18] A. B. Alhassan and T. Duc, "The influence of higher-order disturbance estimation on wind power generation of WECS using SMC with sensorless wind speed estimation," *IEEE Access*, vol. 13, pp. 62179–62197, 2025.

[19] C. Dang, M. Dou, S. Yan, M. Dang, Z. Hua, and D. Zhao, "A sliding mode prediction error compensation of incremental model-based deadbeat predictive current control for SPMSM drives with a sliding mode speed controller," *IEEE Trans. Transport. Electrific.*, vol. 11, no. 4, pp. 9724–9739, Aug. 2025.

[20] X. Sun, Y. Xiong, J. Yang, and X. Tian, "Torque ripple reduction for a 12/8 switched reluctance motor based on a novel sliding mode control strategy," *IEEE Trans. Transport. Electrific.*, vol. 9, no. 1, pp. 359–369, Mar. 2023.

[21] H. Ding, X. Zou, and J. Li, "Sensorless control strategy of permanent magnet synchronous motor based on fuzzy sliding mode observer," *IEEE Access*, vol. 10, pp. 36743–36752, 2022.

[22] B. Tang, W. Lu, B. Yan, K. Lu, J. Feng, and L. Guo, "A novel position speed integrated sliding mode variable structure controller for position control of PMSM," *IEEE Trans. Ind. Electron.*, vol. 69, no. 12, pp. 12621–12631, Dec. 2022.

[23] T. H. Nguyen, T. T. Nguyen, V. Q. Nguyen, K. M. Le, H. N. Tran, and J. W. Jeon, "An adaptive sliding-mode controller with a modified reduced-order proportional integral observer for speed regulation of a permanent magnet synchronous motor," *IEEE Trans. Ind. Electron.*, vol. 69, no. 7, pp. 7181–7191, Jul. 2022.

[24] B. Xu, X. Wang, W. Ji, S. Ding, and T. Liu, "A composite sliding mode control with the modified variable exponential reaching law and super-twisting extended state observer for PMSM," *IEEE Sensors J.*, vol. 25, no. 12, pp. 21284–21294, Jun. 2025.

[25] T.-T. Liu, Y. Tan, G. Wu, and S.-M. Wang, "Simulation of PMSM vector control system based on MATLAB/Simulink," in *Proc. Int. Conf. Measuring Technol. Mechatronics Autom.*, Apr. 2009, pp. 343–346.

[26] J. A. Moreno, "A linear framework for the robust stability analysis of a generalized super-twisting algorithm," in *Proc. 6th Int. Conf. Electr. Eng. Comput. Sci. Autom. Control. CCE*, 2009, pp. 1–6.

[27] Z. Wang, Q. Li, and S. Li, "Adaptive integral-type terminal sliding mode fault tolerant control for spacecraft attitude tracking," *IEEE Access*, vol. 7, pp. 35195–35207, 2019.

TRAN THANH TUYEN received the B.S. and M.S. degrees in electrical engineering from Hanoi University of Science and Technology, Vietnam, in 2008 and 2016, respectively. He is currently pursuing the Ph.D. degree in control science and engineering with Central South University, Changsha, China.

He has been with Quang Ninh University of Industry, Quang Ninh, Vietnam, since 2012. His main research interests include motor control, electrical machines, and power electronics.

JIAN YANG (Member, IEEE) received the Ph.D. degree in electrical engineering from the University of Central Florida, Orlando, in 2008.

He was a Senior Electrical Engineer with Delta Tau Data Systems Inc., Los Angeles, CA, USA, from 2007 to 2010. Since 2011, he has been with Central South University, Changsha, China, where he is currently a Professor with the School of Automation. His main research interests include control applications, motion planning, and power electronics.

DAWEI NI received the B.S. degree in measurement and control technology and instruments from Shandong University of Technology, in 2020, and the M.S. degree in electronic information from Changchun University of Technology, in 2023. Currently, he is pursuing the Ph.D. degree in electronic information with Central South University and concurrently working at Shenzhen Huacheng Industrial Control Co., Ltd., China.

His main research interests include robotics, automation, and control theory.

QILONG LIANG received the B.S. degree in engineering from Hebei University of Science and Technology, in 2012, and the M.S. degree in mechanical engineering from Hohai University, in 2015. He was the Technical Manager for the turbine blade inspection project at Aofanwell Intelligent Technology Company Ltd., from 2015 to 2018. Then, he was a senior application engineer for precise motion control in U.S.-funded company, MKS/Newport, from 2018 to 2023. Since 2023, he has been the Director of the Precision Motion Control Research and Development Department, Maxwell Technology (Zhuhai) Company Ltd., focusing on the development of a high-performance integrated drive-control platform and precise measurement. Also, he is concurrently working toward the Ph.D. degree in Electronic Information at Central South University, Changsha, China.

NGUYEN GIA MINH THAO (Senior Member, IEEE) received the B.Eng. degree (Hons.) in electrical and electronics engineering from Vietnam National University–Ho Chi Minh City University of Technology, Vietnam, in 2009, and the Dr.-Eng. degree in electrical engineering and intelligent control from Waseda University, Tokyo, Japan, in 2015.

From 2015 to 2020, he was a Postdoctoral Researcher with Waseda University and Toyota Technological Institute, Japan. From 2020 to 2023, he was an Assistant Professor with Nagoya University and Toyota Technological Institute. Since 2023, he has been an Associate Professor with Shimane University, Japan, where he is currently the Head of the Electric Motors and Energy Systems Laboratory. His research interests include advanced control methods, electric motors and drives, power electronics, electromagnetic analysis, renewable energy, computational intelligence, and electric vehicles. He has been an Editorial Member of *Journal of Computer Science and Cybernetics*, since 2021. He has been an Associate Editor of IEEE Transactions on Industry Applications, since 2022. He was also a Guest Editor for Special Issues on refereed journals, such as *Sensors*, *Electronics*, and *The Journal of Engineering* (IET).